GeoHealth

RESEARCH ARTICLE
10.1029/2019GH000183

Key Points:
- In 2015, ship emissions increased summer $PM_{2.5}$ and O_3 by 1.4 μg/m^3 and 1.9 ppb, respectively, within the Pearl River Delta (PRD), China
- Ship emissions caused over 2,500 $PM_{2.5}$-related and 1,200 O_3-related premature deaths in the PRD region in 2015
- Implementing an Emission Control Area in the PRD region in 2030 could reduce mortality due to $PM_{2.5}$ and O_3 exposures by 30% and 10%, respectively

Supporting Information:
- Supporting Information S1

Correspondence to:
E. Saikawa,
eri.saikawa@emory.edu

Citation:
Chen, C., Saikawa, E., Comer, B., Mao, X., & Rutherford, D. (2019). Ship emission impacts on air quality and human health in the Pearl River Delta (PRD) region, China, in 2015, with projections to 2030. *GeoHealth*, *3*, 284–306. https://doi.org/10.1029/2019GH000183

Received 17 APR 2019
Accepted 8 JUL 2019
Accepted article online 27 JUL 2019
Published online 30 SEP 2019

Ship Emission Impacts on Air Quality and Human Health in the Pearl River Delta (PRD) Region, China, in 2015, With Projections to 2030

Chen Chen[1,3], Eri Saikawa[1,2], Bryan Comer[3], Xiaoli Mao[3], and Dan Rutherford[3]

[1]Department of Environmental Sciences, Emory University, Atlanta, GA, USA, [2]Department of Environmental Health, Emory University, Atlanta, GA, USA, [3]International Council on Clean Transportation (ICCT), Washington, DC, USA

Abstract Ship emissions contribute to air pollution, increasing the adverse health impacts on people living in coastal cities. We estimated the impacts caused by ship emissions, both on air quality and human health, in 2015 and future (2030) within the Pearl River Delta (PRD) region of China. In addition, we assessed the potential health benefits of implementing an Emission Control Area (ECA) in the region by predicting avoided premature mortality with and without an ECA. In 2015, ship emissions increased $PM_{2.5}$ concentrations and O_3 mixing ratios by 1.4 μg/m^3 and 1.9 ppb, respectively, within the PRD region. This resulted in 466 and 346 excess premature acute deaths from $PM_{2.5}$ and O_3, respectively. Premature mortality from chronic exposures was even more significant, with 2,085 and 852 premature deaths from ship-related $PM_{2.5}$ and O_3, respectively. In 2030, we projected the future ship emissions with and without an ECA, using two possible land scenarios. With an ECA, we predicted 76% reductions in SO_2 and 13% reductions in NO_x from the shipping sector. Assuming constant land emissions from 2015 in 2030 (*2030 Constant* scenario), we found that an ECA could avoid 811 $PM_{2.5}$-related and 108 O_3-related deaths from chronic exposures. Using *2030 Projected* scenario for land emissions, we found that an ECA would avoid 1,194 $PM_{2.5}$-related and 160 O_3-related premature deaths in 2030. In both scenarios, implementing an ECA resulted in 30% fewer $PM_{2.5}$-related premature deaths and 10% fewer O_3-related premature deaths, illustrating the importance of reducing ship emissions.

1. Introduction

Exposure to particulate matter (PM), especially fine PM with an aerodynamic diameter less than or equal to 2.5 μm ($PM_{2.5}$), causes significant adverse health effects (EPA, 2012; Pope III et al., 2002; WHO, 2013). Exposure to tropospheric ozone (O_3) also poses an increased risk of death (Jerrett et al., 2009). Ship emissions are a major source of primary $PM_{2.5}$, including black carbon (BC) and organic carbon (OC), as well as gaseous pollutants such as volatile organic compounds (VOCs), sulfur oxides (SO_x = SO_2 and SO_3), and nitrogen oxides (NO_x = NO and NO_2). VOCs and NO_x can react in the atmosphere in the presence of sunlight and form O_3 (Eyring et al., 2010).

Shipping is an efficient and low-cost means of transportation. Shipping contributes to economic growth in foreign trade, especially in port cities (Frankel, 1989). Shipping transport has seen a steady increase (except in 2009 during the financial crisis), owing to globalization and an increasing size of global-scale trade (UNCTAD, 2018). In 2015, over 10 billion tons of goods (80% of global freight by mass) were exchanged through seaborne trade worldwide (UNCTAD, 2018).

As a result of increased shipping, local air quality in some coastal cities has deteriorated, partly due to ship emissions. Previous studies have found that ship emissions worsened the near-port ambient air quality. According to Corbett et al. (2007), nearly 70% of the ship's exhaust emissions occur within 400 km from the global coastline. Other studies found a 1–45% increase in local $PM_{2.5}$ concentrations due to ship emissions (Chen et al., 2018; Jeong et al., 2017; Liu et al., 2016; Tao et al., 2017; Viana et al., 2014; Yau et al., 2013; Zhang et al., 2017).

Ship emissions also have an impact on human health (Anenberg et al., 2019; Corbett et al., 1999; Corbett et al., 2007; Eyring et al., 2010; Sofiev et al., 2018; Tian et al., 2013). Similarly, Corbett et al. (2007) estimated that ship-related $PM_{2.5}$ were responsible for 60,000 cardiopulmonary and lung cancer deaths worldwide in

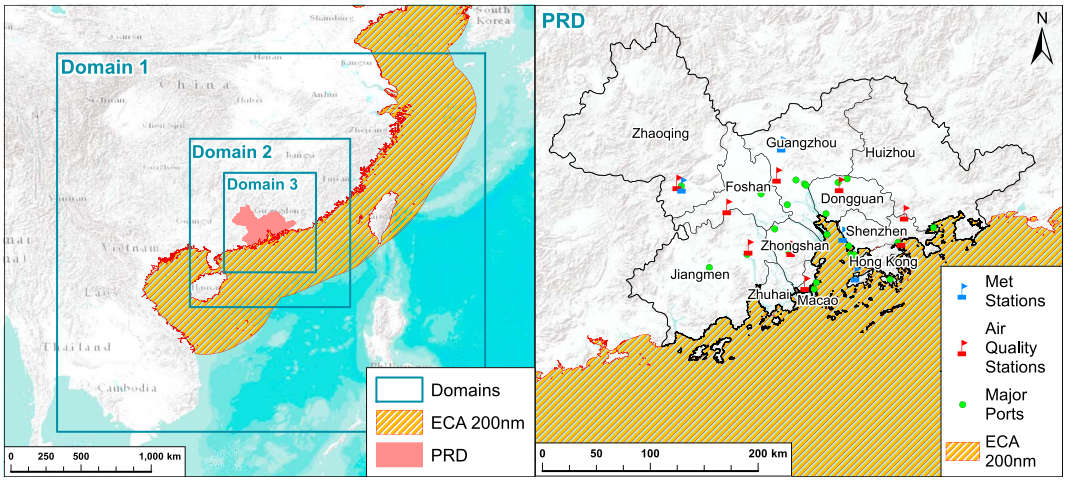

Figure 1. The geographical location of the PRD region (right) and the spatial distribution of ports (green dots), air quality monitoring stations (red), and meteorological stations (blue) inside of the domain 3. The three domain sizes are also shown in the left map. The orange slash area denotes a hypothetical 200 nautical mile (nm) ECA. PRD = Pearl River Delta; ECA = Emission Control Area.

2002. Campling et al. (2013) found that O_3 pollution due to oceangoing ships caused 2.6% of nonaccidental premature deaths in the European Union Member States in 2005. Sofiev et al. (2018) estimated that ship emissions will cause about 1 million premature deaths in 2020 from lung cancer and cardiovascular disease using a log linear concentration-response model. More recently, Anenberg et al. (2019) estimated that international shipping emissions were responsible for 16%, or about 60,000, of global transportation-related premature deaths in 2015.

Without effective emission control policies, as demand for shipping increases, ship emissions will continue to grow. To minimize both the adverse air pollution and health effects from ships, a series of local and global emission control standards have been implemented. The International Convention for the Prevention of Pollution from Ships (MARPOL) Annex VI, which was adopted in 1997 and revised in 2008, included the first large-scale emission control regulations for the international shipping section. Annex VI limits air pollutant emissions from ships, such as SO_x, NO_x, VOCs, and other stratospheric ozone-depleting substances, including halons and a number of chlorofluorocarbons. Emission Control Areas (ECAs) were also established under MARPOL Annex VI to further limit sulfur contents of the fuel in coastal areas, restricting ships to only use fuel with lower than 0.1% sulfur content beginning in 2015. The current ECAs are located in the Baltic Sea, the North Sea, the North American coastal areas, and the U.S. Caribbean Sea. The North American ECA, within 200 nautical miles (nm) of the North American coastline including Canada, also has stringent NO_x emissions standards for ships constructed on or after 1 January 2016. The Baltic Sea and the North Sea ECAs will enforce stringent NO_x emissions standards for ships constructed on or after 1 January 2021.

Several studies have assessed the potential health benefits from the aforementioned ship emissions reduction policies. Winebrake et al. (2009) estimated that 33,500 premature deaths could be prevented annually in the world, if low-sulfur fuel (<0.5% sulfur content) was used by ships in coastal regions, instead of high-sulfur fuels (>2.5%). Sofiev et al. (2018) predicted that the cleaner marine fuels (< 0.5%) could reduce ship-related premature mortality and morbidity by 34% and 54%, respectively in 2020, compared to 3.5% sulfur content fuels. These studies showed that an efficient control policy could render significant health benefits in the global domain.

China, as the world's largest product exporter, has substantial air quality and health risks associated with ship emissions. China owns nearly 5,000 ocean going vessels with a total capacity of over 160 million tons and handled approximately one quarter of the world throughput in its container ports in 2015 (MOT, 2016). The three biggest port clusters in China are the PRD, the Yangtze River Delta, and the Bohai Sea Rim. The PRD port cluster, located in southern China (Figure 1), handled roughly 39% of all exports from China in 2015 (Zhu, 2016). The PRD port cluster has 11 major ports and three of them, Shenzhen, Hong Kong, and

Guangzhou ports, are all ranked among the top 10 largest container ports by TEU (20-ft [6.1 m] Equivalent Unit) volume in the world (WSC, 2014). At the same time, over 58 million residents lived in the central PRD region in 2015 and two megacities, Guangzhou and Shenzhen, had over 13 and 11 million residents, respectively. Therefore, how the emissions from oceangoing ships might pollute the air and threaten the health of local residents is of particular importance.

Many studies have evaluated the impact of ship emissions on local air quality in the coastal cities of China (Chen et al., 2018; Liu et al., 2018; Lv et al., 2018; Zhang et al., 2017), and a few also analyzed their potential health impacts. Liu et al. (2016) found that ship emissions in East Asia resulted in 14,500–37,500 premature deaths per year. In the PRD region, although there is no existing analysis that has included both acute and chronic mortality due to ship emissions, Lin et al. (2016) showed that ship emissions were an important contributor to increased cardiovascular mortality in Guangzhou.

In 2015, the Chinese Ministry of Transports implemented the Domestic Emission Control Area (DECA), which is similar but less stringent than the IMO ECA. DECA limits the sulfur content of the fuels to be less than 0.5% within the 12 nm offshore under a series of time frames. The PRD region, the Yangtze River Delta, and the Bohai Sea Rim are the three major port clusters under the DECA standard. According to the the Chinese Ministry of Transport, SO_x and PM emissions from ships in the three DECA regions would be reduced by 65% and 30% by 2020, respectively, compared to 2015 levels. However, due to its less stringent limitations compared to the IMO ECA, DECA could be less effective in mitigating air pollution than an ECA. To date, a limited number of studies have thoroughly explored the potential benefits that an IMO standard ECA could provide to the coastal cities in China (Liu et al., 2018), but none have yet estimated both air quality and health benefits in the PRD region.

The objectives of this study are to estimate the impacts caused by ship emissions on both air quality and human health, in the past (2015) and in the future (2030) within the PRD region. With the 2015 data, we identify the contributions of ship emissions to ambient pollutant concentrations based on historical emissions and estimate ship-associated mortality from both acute and chronic exposures. We also project future ship emissions in 2030 under both Business As Usual (BAU) and Emission Control Area (ECA) scenarios. Lastly, we assess the potential health benefits for the PRD region by 2030 with ECA implementation by predicting the avoided mortality compared to the BAU scenario. The ECA-related health benefits are compared between *2030 Constant* scenario (constant land emissions as in 2015) and 2030 Projected scenario (projected land emissions by Cai et al., 2018).

2. Methodology

The methodology used in this study is depicted in the flow diagram given in Figure 2.

2.1. Research Area

The research area of this study is the PRD region in China, including the major cities, Guangzhou, Shenzhen, Dongguan, Foshan, Zhongshan, Zhuhai, Jiangmen, Zhaoqing, Huizhou, Macao and Hong Kong (Figure 1). These cities share similar geographical and cultural characteristics. The PRD region is a subtropical monsoon-influenced humid climate, featuring a wet and hot summer and a dry and warm winter (Huang et al., 2012). The average temperature of spring, summer, fall, and winter in the PRD is approximately 20, 28, 25, and 12 °C, respectively. The monthly average rainfall is 250–300 mm during the rainy season from April to September. The monthly average precipitation in the dry season from October to February is approximately 50 mm.

In the central PRD, the highest seasonal average $PM_{2.5}$ concentration was observed in winter (55.6 μg/m^3) and the season with the lowest concentration was in summer (23.4 μg/m^3; Zhang & Cao, 2015). Due to the increasing attention from local governments and emission control policies, the annual average $PM_{2.5}$ concentration was reduced from 79 μg/m^3 in 2007 to 46 μg/m^3 in 2016 (Guangdong-Hong Kong-Macao Pearl River Delta Regional Air Quality Monitoring Network, 2017).

On the other hand, the annual average ground-level O_3 mixing ratio increased from 24 ppb in 2006 to 29 ppb in 2014 (Guangdong-Hong Kong-Macao Pearl River Delta Regional Air Quality Monitoring Network, 2014). O_3 mixing ratio in downwind rural areas is usually higher than those in the urban areas. O_3 mixing ratio is represented by the daily maximum 8-hr average mixing ratio for a given day, which is derived from the

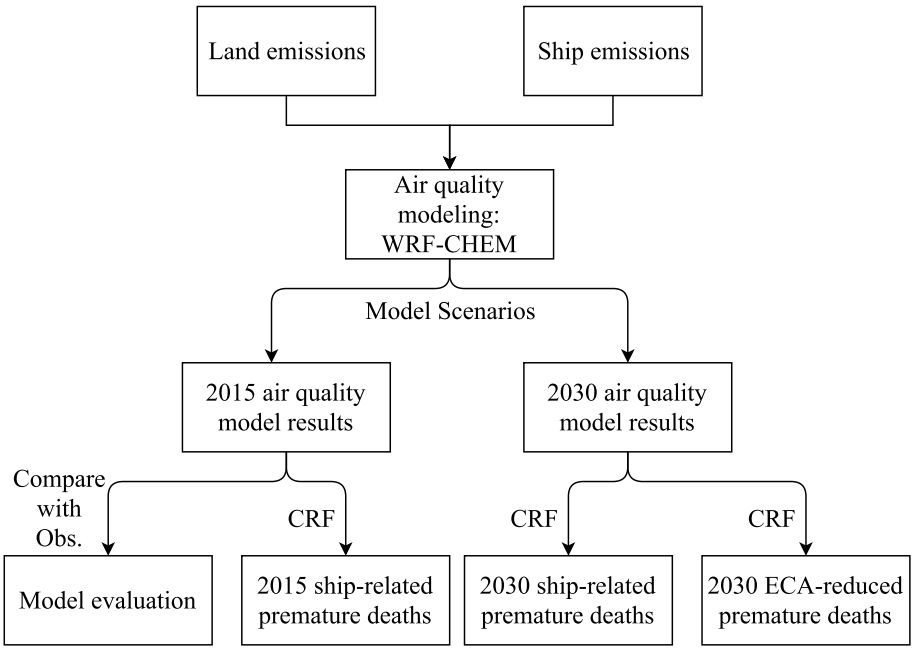

Figure 2. A schematic representation of the methodology used in this study. WRF-Chem = Weather Research and Forecasting model coupled with Chemistry; CRF = concentration-response function.

highest of the 17 consecutive 8-hr averages. High daily maximum 8-hr average O_3 is found in the summer from June to August, while it is low in the winter from December to February.

In 2015, over 58 million residents lived in the central PRD region (GDstats, 2016) and two megacities, Guangzhou and Shenzhen, had over 13 and 11 million residents in 2015, respectively. There are over 20 ports located in the PRD region and eight of them surpassed 70 million tons of cargo throughput in 2015 (Zhu, 2016). In the United States, on the other hand, only seven ports surpassed 70 million tons of cargo throughput in the same year (IWR, 2016).

2.2. Air Quality Simulations

We used the regional chemical transport model Weather Research and Forecasting model coupled with Chemistry (WRF-Chem; Grell et al., 2005) version 3.5 for the ambient air quality estimation. The WRF-Chem simulated air quality within the three domain sizes, all centered at the PRD region (Figure 1). The largest model domain covers the half of Eastern China and neighboring South Asian Countries, with a 27 × 27-km horizontal grid spacing. Two nested domains have finer resolutions of 9 × 9 km and 3 × 3 km, respectively. All three domains have 31 vertical levels, from the surface to 50 hPa. The time period of the model simulation was July 2015, with five spin-up days from 27 June to 30 June. WRF-Chem integrates all prognostic meteorological, chemical, and aerosol variables at each time step and then calculates how these variables change in response to various forcing and advections between the grid cells while conserving the overall mass, energy, and momentum of the system. The time steps used were 120, 40, and 24 s for three domains from coarse to fine resolution.

We used the Regional Acid Deposition Model version 2 (Stockwell et al., 1990) for the gas phase chemical mechanism, to predict the highly nonlinear O_3, sulfate, nitric acid, and hydrogen peroxide concentrations under various atmospheric conditions. For PM, we used the Modal Aerosol Dynamics Model for Europe with the Secondary Organic Aerosol Model (MADE/SORGAM; ; Ackermann et al., 1998; Schell et al., 2001). MADE/SORGAM takes into account aerosol dynamics, including formation (i.e., condensation, nucleation, and coagulation), transport, dry deposition, and aerosol-cloud interaction. MADE/SORGAM further predicts the mass of several particulate phase species, including sulfate, ammonium, nitrate, sea salt, dust, BC, OC, and secondary organic aerosols in the three lognormal aerosol modes (Aitken, accumulation, and coarse).

Photolysis rates are obtained from the Fast-J photolysis scheme (Wild et al., 2000). We used the 6-hr temporal resolution National Center for Environmental Prediction Global Forecast System gridded data as the model meteorological inputs. The simulated horizontal winds, temperature, and humidity were nudged to the respective meteorological fields. We also used initial and lateral boundary conditions from the global chemical transport model, the global Model for Ozone and Related Chemical Tracers 4 (Emmons et al., 2010), to account for the initial and background chemical concentrations.

To evaluate the model's meteorological performance, we compared the simulated air temperature at 2 m (2-m temperature), wind speed, wind direction, and relative humidity with observed values, taken from the National Oceanic and Atmospheric Administration National Climatic Data Center land-based stations (NCEI, 2018). Only four cities, Guangzhou, Shenzhen, Zhaoqing, and Hong Kong, had data for 2015; thus, we chose the observed data from each of these cities to evaluate the model results. We also evaluated the model performance of air pollutant concentrations at nine government-controlled monitoring sites in the PRD region, including Guangzhou, Shenzhen, Zhuhai, Foshan, Zhongshan, Jiangmen, Dongguan, Huizhou, and Zhaoqing. The locations of both meteorological and air quality stations are shown in Figure 1. Based on the coordinates of these monitoring sites, we retrieved their located grids under the smallest domain (3×3 km) and compared the model results on the grid to the observed results.

The model performance was determined by statistical metrics, including the correlation coefficient (r), the normalized mean bias (NMB), the normalized mean error (NME), the mean fractional bias (MFB), the mean fractional error (MFE), and the root-mean-square error between the observed measures and modeled outputs (Chang & Hanna, 2004). We evaluated the model performance of $PM_{2.5}$ based on the standards developed by Boylan and Russell (2006), which set the performance goals for $PM_{2.5}$ at MFB less than or equal to $\pm$30% and MFE less than or equal to 50%. The performance criteria for $PM_{2.5}$ were set at MFB less than or equal to $\pm$60% and MFE less than or equal to 75%. For O_3, both MFB and MFE were set at less than or equal to $\pm$15% and 35%, as recommended by Morris et al. (2007).

2.3. Emission Scenarios

We used the Multiresolution Emission Inventory of China (MEIC; http://www.meicmodel.org) for 2015 anthropogenic emissions in China, other than those from ships. For emissions for the rest of the regions in the domain out of China, we used the Regional Emission Inventory in ASia version 2 (REAS; Kurokawa et al., 2013). Both MEIC and REAS inventories provide emissions of major primary and secondary air pollutant precursors, including NO_x, SO_2, VOCs, NH_3, CO, and PM. PM in both inventories are classified into BC, OC, $PM_{2.5}$ and PM_{10}. We used the Fire INventory from the National Center for Atmospheric Research for the year 2015 (Wiedinmyer et al., 2011) for biomass burning emissions and the Model of Emissions of Gases and Aerosols from Nature version 2.1 (MEGAN v2.1; Guenther et al., 2012) for biogenic emissions based upon the weather and land use data. WRF-Chem calculated the dust and sea salt emissions online by using the dust transport model (Shaw et al., 2008) and sea salt schemes (Gong, 2003). Also added were the aircraft emissions of BC, CO, OC, $PM_{2.5}$, NO_x, and SO_2 from the Hemispheric Transport of Air Pollution emissions inventory (HTAP_v2.2; Janssens-Maenhout et al., 2015).

In 2030, we ran scenarios under two land emission inventories, 2015 land emissions (referred as 2030 Constant scenario below, as we assumed no change in emissions from 2015), and 2030 projected land emissions (referred as 2030 Projected scenario below, developed by Cai et al., 2018). The 2030 projected land emissions considered additional measures that could potentially reduce anthropogenic emissions on the land. The model had the same MEGAN v2.1 biogenic emissions as in 2015, as we assumed no major changes in land cover in 2030, but we ignored biomass burning emissions, which would be negligible in July, compared to other future emission sources.

We created six emissions scenarios for this study (Table 1). The 2015 scenarios (S0 and S1) used the same land source emissions from the MEIC and REAS inventories. Based on whether ship emissions were added, S0 and S1 were called *2015 Without Ship* and *2015 With Ship*. We created four scenarios for 2030. The *2030 BAU Constant* scenario and *2030 ECA Constant* scenario (S2 and S3) also used the same 2015 land source emissions. The *2030 BAU Projected* scenario and *2030 ECA Projected* scenario (S4 and S5) adopted the 2030 projected land emissions. Different ship emissions are explained more in detail below.

To find the largest possible impacts on air quality from ship emissions, we modeled the month of July, which is the monsoon season and when southeastern winds transport ship emissions from the sea to the land

Table 1
Scenarios Used in This Study for Running the Air Quality Model

Scenarios	Scenario name	Description	Emission control policies for ships
S0	2015 without ship	2015 land emissions	N/A
S1	2015 with ship	2015 land emissions plus 2015 ship emissions	PM and SO_2: None NO_x: Tier II ship engine
S2	2030 BAU constant	2015 land emissions plus 2030 BAU ship emissions	PM and SO_2: Global: IMO sulfur cap, China: DECA 2.0 NO_x: Tier II ship engine
S3	2030 ECA constant	2015 land emissions plus 2030 ECA ship emissions	PM and SO_2: Global: IMO sulfur cap, China: ECA NO_x: Tier III ship engine for ships built after 2025
S4	2030 BAU projected	2030 projected land emissions plus 2030 ECA ship emissions	PM and SO_2: Global: IMO sulfur cap, China: DECA 2.0 NO_x: Tier II ship engine
S5	2030 ECA projected	2030 projected land emissions plus 2030 ECA ship emissions	PM and SO_2: Global: IMO sulfur cap, China: ECA NO_x: Tier III ship engine for ships built after 2025

Note. BAU = Business As Usual; PM = particulate matter; ECA = Emission Control Area.

(Lu et al., 2009). During this season, impacts from ship emissions toward the PRD cities most likely reach maximum. Some studies have also shown that July has the highest contributions of ship emissions toward land in China (Chen et al., 2018; Liu et al., 2018).

2.4. Ship Emissions

2.4.1. Ship Emissions for 2015

The 2015 ship emission estimates are derived from the International Council on Clean Transportation's (ICCT) Systematic Assessment of Vessel Emissions (SAVE) model. The ICCT's 2017 report (Olmer et al., 2017) provides a detailed methodology. The model systematically estimates ship emissions using a bottom-up method by coupling the Automatic Identification System (AIS) data and the ship characteristic data (made available by IHS Fairplay). AIS data include the hourly location, speed, and draught for individual ships. Combined with ship-specific characteristics, the SAVE model estimates a ship's energy demand and emissions.

The SAVE model calculated the hourly emissions for each ship and then aggregated all ships within the domain to find the overall emissions at each hour, using the following equation:

$$E_{i,j} = \sum_{t=0}^{t} (P_{ME_i} \times LF_{i,t} \times EF_{ME_{i,k,l,m}} + D_{AE_{p,i,t}} \times EF_{AE_{j,k,l,m}} + D_{BO_{p,i,t}} \times EF_{BO_{j,m}}) \quad (1)$$

where E is emissions (g/hr), P_{ME} is main engine power (kW), LF is main engine load factor (%), EF_{ME} indicates main engine emission factor (g/kWh), D_{AE} indicates auxiliary engine power demand (kW), EF_{AE} is auxiliary engine emission factor (g/kWh), D_{BO} indicates boiler power demand (kW), and EF_{BO} indicates boiler emission factor (g/kWh). *i* indicates each ship, *j* indicates each pollutant, *k* indicates engine type (two-stroke or four-stroke engine), *l* indicates engine tier (Tier I, Tier II, and Tier III), *m* indicates fuel type (residual fuel, distillate fuel, LNG, methanol, coal, or nuclear), *p* indicates operating phase (cruise, maneuvering, anchor, or berth), and *t* indicates operating hour. We used BC, CO, PM, SO_2, NO_x, and nonmethane VOC emissions estimates from the SAVE model as the air quality model input.

We also estimated the 2015 fuel consumption ($FC_{i,2015}$) by dividing the CO_2 emissions (outputted from the SAVE model) by the carbon intensity of the specific fuel. Carbon intensity is 3.114 g CO_2 for residual fuel,

3.206 g CO_2 for distillate fuel, and 2.75 g CO_2 for LNG. There are no ships running on coal, nuclear, or methanol in 2015, based on the AIS data. The $FC_{i,2015}$ was used to project 2030 fuel consumption and ship emissions, as explained in the following section.

2.4.2. Ship Emissions for 2030

The 2030 ship emissions are projected based on the 2015 gridded ship emissions. We projected future ship emissions in 2030 under two scenarios: Business as usual (referred to as 2030 BAU) and with a PRD 200-nm ECA scenario (2030 ECA; Figure 1, orange slash area). In the BAU scenario, we considered only the existing policies that are currently implemented or planned to be in force by 2030, whereas in the ECA scenario, we modeled a 200-nm-wide ECA in the PRD region.

Two factors were considered to project the future emissions of pollutant j for ship i in 2030 ($E_{i,j,2030}$): fuel consumption and emission factors. The conceptual equation is written as follows:

$$E_{i,j,2030} = \sum (FC_{i,2015} \times SF_{2030FC,i}) \times (EF_{i,j,2015} \times SF_{2030EF,j}) \quad (2)$$

where $FC_{i,2015}$ is the fuel consumption in 2015 (g), $SF_{2030FC,i}$ is the scale factor used to project the 2030 fuel consumption, $EF_{i,j,2015}$ is the emission factor in 2015, and $SF_{2030EF,j}$ is the scale factor used to project the 2030 emission factor. In short, $SF_{2030FC,j}$ is based on the expected change of the future shipping demand, and $SF_{2030EF,j}$ is estimated due to the change of future emission control policies. The $FC_{i,2015}$, as introduced in the previous section, is obtained from the SAVE model. The $EF_{i,j,2015}$ for each pollutant is described in Tables S1 and S2 in the supporting information. In our 2030 ship emissions, $SF_{2030FC,i}$ was the same for both 2030 BAU and 2030 ECA but the two had different $SF_{2030EF,j}$ values.

To estimate the $SF_{2030FC,i}$ for the two scenarios, we mainly considered three factors in 2030: fleet turnover, trade volume, and new ship Energy Efficiency Design Index (EEDI) requirements (described later in the section). $SF_{2030FC,i}$ was calculated as follows:

$$SF_{2030FC,i} = \frac{SF_{\text{power}} \times SF_{\text{TradeVolume}} \times SF_{\text{EEDI}}}{SF_{\text{dwt}}} \quad (3)$$

where SF_{power} is the scale factor for engine power, $SF_{TradeVolume}$ is the scale factor for trade volume, SF_{EEDI} is the scale factor for EEDI, and SF_{dwt} is the scale factor for cargo carrying capacity, called deadweight tonnage. A future fleet turnover model designed by ICCT provided SF_{power} and SF_{dwt}. The model was built based on the following assumptions:

- The average lifetime for an oceangoing vessel is 25 years.
- The total number of vessels in the world will not change.
- The average ship size will increase by 0.3–6% depending on ship types.
- The average main engine power will increase by 2–8% depending on ship types.
- The average deadweight tonnage will increase by 0.5–12% depending on ship types.
- The overall fuel efficiency will increase as EEDI improves.

We estimated the 2030 trade volume ($SF_{TradeVolume}$) based on historical data (2006–2015) published by the United Nations Conference on Trade and Development, which summarizes seaborne trade volume by region and by major cargo type annually. In this study, linear extrapolation of the historical data from 2006 to 2015 helped project the 2030 trade volume. Projections were based on the following assumptions:

- The world seaborne trade will continue growing because of increasing globalization and decreasing transportation cost.
- Asia will become the center of international trade (SISI, 2015).
- Containerized cargo and bulk cargo are still showing good momentum to grow but likely with a less aggressive expansion rate compared to previous years.
- LNG transport will quickly catch up with the other dominant cargoes, while crude oil trade will slow down in the long term.

With the projected trade volume for 2030, we found the compound annual growth rate as well as the overall growth rate over the 15-year period. The trade volume growth rates specific to cargo type can be uniquely tied to ship classes. For example, a class such as bulk carriers only carry major dry bulk cargo, like coal, grain, or ore, while oil tankers only carry crude oil and petroleum products. For ship classes whose corresponding

cargo does not have specific forecast numbers, the overall trade growth rates for Asian developing countries were used instead.

The EEDI, set forth by IMO, mandates that ships built after a certain date need to gradually become more energy efficient than the baseline fleet in terms of gCO_2/dwt-nm (MEPC.203(62), 2011). With the goal being to reduce greenhouse gas emissions from shipping, EEDI mandates that ships become more efficient by improving performance of the ship itself. EEDI has five components: shaft power, specific fuel consumption (SFC), CO_2 emission rate, deadweight tonnage, and design speed. Controlling for the other four components, our SF_{EEDI} can approximate the impact of engine fuel efficiency improvement over time. To account for ships becoming more efficient over time due to the EEDI, we assumed a 20% reduction in the carbon intensity of the shipping fleet in 2030 compared to 2015. Thus, the scale factor for EEDI (SF_{EEDI}) is 80% in the above equation (3).

The SF_{2030EF_j} is determined by the associated policies, and because an ECA mainly targets a few pollutants, such as PM, SO_2, and NO_x, the emission factors for those three pollutants will be primarily affected, while others such as CO and NMVOC will not. The emission factor for BC will be affected as well, as using ECA-compliant fuels tend to reduce BC emissions (Comer et al., 2017).

The fuel-based emission factor for SO_2 is determined by the sulfur content of fuels assuming that 97.753% of the fuel sulfur was converted to SO_2 and taking into account the molecular weight difference between SO_2 and sulfur, as described below

$$EF_{SO_2}\left(\frac{SO_2\,(g)}{\text{fuel}\,(g)}\right) = 2 \times 0.97753 \times \%\text{Fuel Sulfur Content} \tag{4}$$

and %FuelSulfurContent is different under 2030 BAU and 2030 ECA scenarios. Current global average sulfur content for marine fuel is approximately 2.5% m/m. Under the 2030 BAU scenario, we considered two policies: the IMO fuel sulfur cap and DECA 2.0. The IMO fuel sulfur cap starting in 2020 will require all IMO-regulated vessels to use fuel with a maximum of 0.5% sulfur content globally. This cap would cause an 80% reduction in SO_2 emission factor, under the BAU scenario, compared to current fuel sulfur contents. DECA 2.0 refers to the upgraded DECA starting in 2019. Under the DECA 2.0 region, all ship fuels must be a max of 0.5% in sulfur content, according to the current DECA (or DECA 1.0); in addition, all ships berthing in China or traveling within 12-nm coastline of Hainan Province will be required to use marine fuel with a max of 0.1% sulfur content (At the time of modeling, the DECA 2.0 proposal was under public review. When it was released in December 2018, the requirement for fuel used while berthing with a max 0.1% sulfur content was removed but we still kept the original proposal to consider the most stringent regulation possible.) Thus, when berthing or operating near Hainan Province, there will be a 96% reduction in the SO_x emission factor in the 2030 BAU scenario.

Under the 2030 ECA scenario, in addition to the policies that have already been mentioned for the BAU, we assumed that a 200-nm ECA will be applied in the PRD coastline region. An ECA would require a maximum 0.1% fuel sulfur content; thus, a 96% reduction of the SO_2 emission factor would be applied to the whole region.

The PM emission factor is also related to the fuel sulfur content. Thus, all aforementioned policies to reduce fuel sulfur content will have a positive spillover effect on PM as well. PM emission factors are ship specific because they are also dependent on the SFC by ship classes; based on fuel (residual (HFO) or distillate fuel (MDO/MGO)), we applied different equations to calculate them

$$EF_{PM} = \begin{cases} 1.35 + SFC \times 7 \times 0.02247 \times (\%\text{Fuel Sulfur Content} - 0.0246) \times SFC, & HFO \\ 0.23 + SFC \times 7 \times 0.02247 \times (\%\text{Fuel Sulfur Content} - 0.0024) \times SFC, & MDO/MGO \end{cases} \tag{5}$$

The type of engine installed on ships determines the NO_x emission factor. Thus, the projection of the NO_x emission factor is based on the fleet's age distribution in 2030. The IMO has also assigned several tiers for marine diesel engines under MARPOL Annex VI (Table S3). To project the 2030 NO_x emission factor, it was assumed that all the new ships built after 2025 would follow the up-to-date Tier III engine standards. For the rest of the ships built before 2025, they would only meet Tier II within the ECA region. The commonly accepted Tier III compliance technology is to install an after-treatment device, such as Selective Catalytic Reduction, which reduces NO_x to nitrogen gas (N_2) when urea or ammonia is injected in the exhaust gas.

Table 2
Health Outcomes and Risk Functions Used to Calculate the Burden of Diseases Associated With the Exposure to $PM_{2.5}$ and O_3

Outcome and exposure metric	Relative risks (95% CI)	Reference
All cause (unnatural) mortality from short-term exposure to $PM_{2.5}$	1.0176 (1.0147, 1.0206)	Lin et al. (2016)
Cardiovascular disease (CVD) mortality from short-term exposure to $PM_{2.5}$	1.0219 (1.0180, 1.0259)	Lin et al. (2016)
Respiratory infection (RESP) from short-term exposure to $PM_{2.5}$	1.0168 (1.010, 1.0237)	Lin et al. (2016)
All cause (unnatural) mortality from short-term exposure to O_3	1.0081 (1.0063, 1.010)	Tao et al. (2011)
Cardiovascular disease (CVD) mortality from short-term exposure to O_3	1.0101 (1.0071, 1.0132)	Tao et al. (2011)
Respiratory infection (RESP) from short-term exposure to O_3	1.0133 (1.0089, 1.0176)	Tao et al. (2011)
Ischemic heart disease (IHD) from long-term exposure to $PM_{2.5}$		
Chronic obstructive pulmonary disease (COPD) from long-term exposure to $PM_{2.5}$	IER	
Cerebrovascular disease (CEV) from long-term exposure to $PM_{2.5}$	* Depends on specific concentrations and age groups.	2015 GBD study
Lung cancer (LC) from long-term exposure to $PM_{2.5}$		
Respiratory infection (RESP) from long-term exposure to $PM_{2.5}$	1.009 (0.982, 1.04)	Tao et al. (2011)
Ischemic heart disease (IHD) from long-term exposure to O_3	1.015 (1.003, 1.026)	Jerrett et al. (2009)
Respiratory infection (RESP) from long-term exposure to O_3	1.029 (1.010, 1.048)	Jerrett et al. (2009)
Cardiovascular (CVD) mortality from long-term exposure to O_3	1.011 (1.003, 1.023)	Jerrett et al. (2009)

Exhaust Gas Recirculation can also be used to control NO_x from larger, two–stroke marine engines. The overall impact of ECA NO_x requirements was calculated on a per ship basis and summarized for each ship class.

BC emission factors depend on the fuel type. ECA fuel sulfur regulations will be mostly achieved by switching to cleaner fuels. BC emission factors associated with different fuel types were taken from Comer et al. (2017). The emission factors for CO and NMVOC were unchanged from the 2015 emission factors. Thus, based on the potential ship emission policies, we designed a $SF_{2030EF,j}$ for each pollutant j as summarized in Table S4. The emission factors of pollutants in 2030 are the products of emission factors in 2015 and their respective $SF_{2030EF,j}$.

2.5. Health Impact Estimation

The health impacts due to ship-caused $PM_{2.5}$ and O_3 increases were estimated for both acute (short-term) and chronic (long-term) mortality. Because of computational challenges associated with modeling multiple years of air quality, we used our 1-month simulation to estimate both acute and chronic health impacts from ship emissions. We assumed that the difference in air quality from our model simulations would hold for a longer term. The relative risk (RR) is the ratio of the incidence of death among those exposed by the extra pollution ($PM_{2.5}$ or O_3 in this study), due to ship emissions, to the nonexposed population, as summarized in Table 2.

For the acute mortality, we calculated the total number of deaths in all-cause, cardiovascular disease (CVD), and respiratory infection (RESP) for both $PM_{2.5}$ and O_3. The RR due to pollution for each health endpoint was derived from the pooled estimate of the increased mortality due to 10 $\mu g/m^3$ increase of $PM_{2.5}$ or 10 ppb O_3 concentrations from the PRD-specific epidemiological time series studies by Lin et al. (2016) and Tao et al. (2011).

For the chronic mortality due to $PM_{2.5}$ exposures, the RRs can vary with different $PM_{2.5}$ concentrations. Thus, we adopted the long-term Integrated Exposure Response (IER) function to find the RRs under different $PM_{2.5}$ concentrations, which is the most recognized method to estimate chronic $PM_{2.5}$-related mortality. The IER function for each health point was developed by Burnett et al. (2014) and is widely used to estimate the global burden of disease attributable to $PM_{2.5}$ exposure over the entire global exposure range. The IER model is written as

$$RR(c) = \begin{cases} 1, & c < c_{cf} \\ 1 + \alpha\{1 - e^{[-\gamma(c-c_{cf})]^{\delta}}\}, & c \geq c_{cf} \end{cases} \quad (6)$$

where c is the exposure to $PM_{2.5}$ and c_{cf} is the counterfactual concentration, below which no additional risk is assumed. The parameters (i.e., α, γ, and δ) for each health endpoint are decided by fitting a curve to RR

data taken from studies on ambient air pollution, second-hand tobacco smoke, household solid cooking fuel, and active smoking. Since there are only few cohort studies performed in China, and none of them has been further validated, the IER functions are currently regarded as the best estimate of the long-term mortality in China. The IER functions are developed for causes of mortality, including ischemic heart disease (IHD), cerebrovascular disease (CEV), chronic obstructive pulmonary disease (COPD), and lung cancer (LC).

Due to the lack of studies for the chronic mortality due to O_3 exposure, we simply adopted RRs from a cohort study by Jerrett et al. (2009) for CVD, RESP and IHD. Unlike RRs developed by the IER model, a single set of RRs is used for all concentrations and age groups, and therefore, a higher uncertainty might remain in the O_3 chronic mortality estimation than in the $PM_{2.5}$ chronic mortality estimation.

Using the following equation, we first derived the concentration-response function coefficients from the RR:

$$\beta = \frac{\ln(RR)}{\Delta c} \tag{7}$$

where RR is the relative risk, β is the coefficients of exposure-response functions, Δc is the unit of increased air pollutant concentrations (10 μg/m^3 or 10 ppb in most time-series studies). Either acute or chronic mortality was then estimated by the following log linear model, which links the air pollutant concentration difference to health endpoints

$$\Delta y = y_0\{1 - e^{-\beta(C_1 - C_0)}\} \times Pop \tag{8}$$

where Δy is the increased incidence of each health endpoint due to ship emissions in 2015 or the decreased incidence due to ECA implementation in 2030, y_0 is the base incidence rate of each health endpoint, β is the coefficient of exposure-response functions, C_1 is 2015 With Ship concentration or 2030 BAU concentration (from either land emission scenario), and C_0 is 2015 without ship concentration or 2030 ECA (from either land emission scenario) concentration. C_1-C_0 is either the increased air pollutant concentration due to ship emissions in 2015 ($\Delta C_{\text{Ship Related}}$) or the decreased concentration due to ECA implementation in 2030 (ΔC_{ECA}), as shown in equations (9) and (10).

$$\Delta C_{\text{Ship Related}} = C_{2015\ \text{With Ship}} - C_{2015\ \text{Without Ship}} \tag{9}$$

$$\Delta C_{\text{ECA}} = C_{2030\ \text{BAU}} - C_{2030\ \text{ECA}} \tag{10}$$

We obtained the baseline incidence of short-term all-cause, CVD, and RESP for the six main cities in PRD from the Guangdong Provincial Center for Disease Control and Prevention (Lin et al., 2016). Due to a lack of city-specific baseline incidence rates for chronic diseases, we applied the provincial baseline incidence rates in 2015 (personal communication with Health Effects Institute on Oct. 2018), to all cities in Guangdong Province, and applied the stand-alone rates for Hong Kong because of its special cultural and governmental settings from the mainland China. For 2030 scenarios, only chronic mortality was predicted due to the lack of baseline incidence data.

Pop is the population associated to each 3 × 3-km grid. The Gridded Population of the World version four (v4) provides the 2015 population gridded data in 1 × 1-km horizontal resolution (NASA, SEDAC), and the grid cells were aggregated to match with the air pollution grid cells. We obtained the population projections for 2030 from the United Nations Economic and Social Commission for Asia and the Pacific (UN ESCAP) Probabilistic Population Projections. Based on the estimation from the UN Department of Economic and Social Affairs in their 2017 revision, the median population projection for mainland China (excluding Macao, Hong Kong, and Taiwan) for 2030 is 1.44 billion, compared to 1.40 billion in 2015. Since no gridded 2030 population data were available, we used the gridded 2015 population, combined with the ratio of the total population in 2030 to the base year 2015 for each 3 × 3-km grid. Thus, all the death incidences were estimated in each 3 × 3-km grid and then aggregated within each city or the whole PRD region.

3. Results

We first introduce emissions estimates in section 3.1, for both land and ship, and present the results from air quality modeling using various scenarios in section 3.2. We then show results for air quality and health impacts from ship emissions in sections 3.3 and 3.4. The results will be further discussed in section 4.

Table 3
Summary Emissions for Different Scenarios Used in the Model

Unit: (kt/year)	2015 and 2030 constant land emissions		2030 projected land emissions		Ship emissions within PRD coastal region		
	China	PRD	China	PRD	2015	2030 BAU	2030 ECA
$PM_{2.5}$	9,237	158	2,957	82	11.3	9.9	4.3
SO_2	18,335	350	9,710	384	89.5	27.0	6.4
NO_x	25,702	669	8,188	489	141.9	197.9	172.3

Note. The left four columns account for two land emissions scenarios Within China or PRD only and the right three columns account for three ship emissions scenarios within PRD coastal region. PRD = Pearl River Delta; BAU = Business As Usual; ECA = Emission Control Area.

3.1. Emissions

Table 3 describes the emissions of $PM_{2.5}$, SO_2, and NO_x for two land scenarios and three ship scenarios. In 2015, there were 9,237 kt/year of $PM_{2.5}$, 18,335 kt/year of SO_2, and 25,702 kt/year of NO_x emitted in China from all the major land sources (e.g., power plant, residential, land transportation, agriculture, and industry). Within the PRD region, land-based sources emitted 158 kt/year of $PM_{2.5}$, 350 kt/year of SO_2, and 669 kt/year of NO_x in the same year, accounting for about 1.7%, 1.9%, and 2.6% of total emissions in China.

We assumed that the annual land-source emissions would fall between 2015 and 2030 projected emissions by Cai et al. (2018). China as a whole, the primary $PM_{2.5}$, SO_2, and NO_x land emissions would be reduced by 68.0%, 47.0%, and 68.1%, respectively, between 2015 and 2030 projected emissions (Table 3). In the PRD, the projected emissions predicted 82 kt/year of $PM_{2.5}$, 384 kt/year of SO_2, and 489 kt/year of NO_x emitted. Both $PM_{2.5}$ and NO_x emissions are expected to reduce under the 2030 Projected scenario, while the SO_2 show a small increase. The $PM_{2.5}$ and NO_x emission reduction rates were 48.1% and 26.9% and were smaller than the national reduction rates. These results might indicate that the 2015 emissions in PRD are already reduced and the future emission control mainly result in the rest of China rather than from the PRD region.

Ship emissions varied greatly among the three scenarios (2015, 2030 BAU, and 2030 ECA), as summarized in Table 3. Our results illustrate the potential difference in ship emissions within the 200-nm ECA region in the PRD. In 2015, within the 200-nm ECA region, we estimated 11.3 kt/year of $PM_{2.5}$, 89.5 kt/year of SO_2, and 141.9 kt/year of NO_x by ships. Ship-emitted $PM_{2.5}$, SO_2, and NO_x accounted for 7%, 20%, and 17% of all emissions in the entire PRD area (PRD + 200 nm).

For the 2030 BAU scenario, we estimated 9.9 kt/year of $PM_{2.5}$, 27.0 kt/year of SO_2, and 197.9 kt/year of NO_x emissions from ships within the 200-nm ECA region. Compared to the 2015 ship emissions, this is a 12% decrease for $PM_{2.5}$, a 70% decrease for SO_2, but a 39% increase for NO_x. Under the 2030 ECA scenario, we estimated that 4.3 kt/year of $PM_{2.5}$, 6.4 kt/year of SO_2, and 172.3 kt/year of NO_x would be emitted from ships

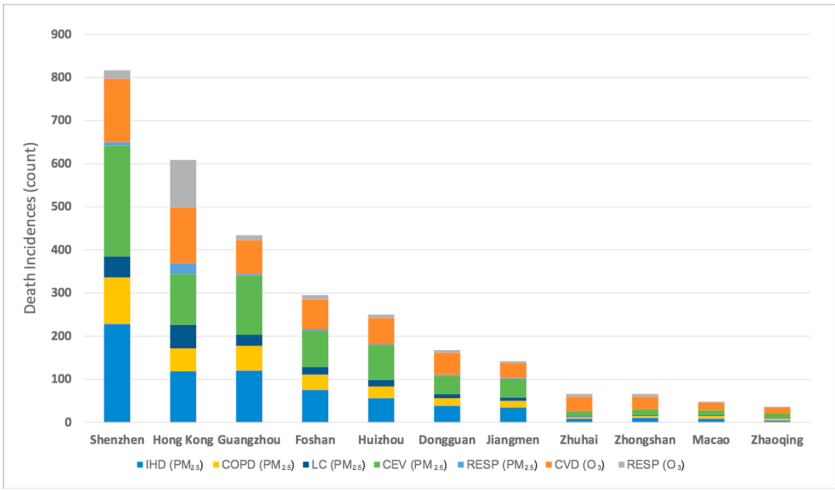

Figure 3. Spatial distribution of $PM_{2.5}$, SO_2, and NO_x emissions from ships in July under the three ship scenarios (unit: tons/100 km^2).

Table 4
Summary Statistics for the Four Meteorological Variables (Temperature, Wind Speed, Wind Direction, and Relative Humidity) Between Modeled and Observed in Four Cities of the PRD Region in July 2015

Variable	Site	NMB (%)	NME (%)	MFB (%)	MFE (%)	*r*	RMSE
2-m temperature	Guangzhou	0.3	0.3	0.1	0.1	0.9	1.2
	Shenzhen	0.2	0.3	0.1	0.1	0.8	1.1
	Zhaoqing	−0.3	0.4	−0.1	0.1	0.7	1.6
	Hong Kong	0	0.2	0	0.1	0.8	0.9
10-m wind speed	Guangzhou	-15	17.6	−4.4	5.1	0.9	0.6
	Shenzhen	−36.4	36.4	−11.2	11.2	0.8	2
	Zhaoqing	31.6	39.9	5.9	8	0.5	1
	Hong Kong	−35.9	35.9	−11	11	0.8	1.9
10-m wind direction	Guangzhou	−9.8	21	−2.7	5.6	0.5	45.7
	Shenzhen	−0.8	11.9	−0.7	3.2	0.8	30.7
	Zhaoqing	−5.9	21.1	−0.8	5.6	0.5	47.3
	Hong Kong	11.2	17.8	2.2	4.1	0.6	46.4
Surface relative humidity	Guangzhou	−15.9	16.4	−4.7	4.9	0.5	17
	Shenzhen	−12.3	15.1	−3.8	4.5	0.6	15.9
	Zhaoqing	−1.6	9.1	−0.6	2.4	0.5	10.1
	Hong Kong	−2.6	11.2	−1.1	3.1	0.7	11.2

Note. PRD = Pearl River Delta; NMB = normalized mean bias; NME = normalized mean error; MFB = mean fractional bias; MFE = mean fractional error; RMSE = root-mean-square error.

within the 200-nm ECA region, resulting in 57%, 76%, and 13% decrease of $PM_{2.5}$, SO_2, and NO_x, respectively, from the 2030 BAU scenario. Comparing ship emissions between 2030 ECA and 2015 ship emissions, we found that $PM_{2.5}$ and SO_2 emissions would decrease by 62% and 93%, respectively, but NO_x would still increase by 21%. The cause of these differences will be elaborated in the discussion section. Compared to 2030 Projected land emissions, ship emissions would be about 25% of all NO_x emissions in the PRD region in 2030.

Figure 3 illustrates the gridded ship emissions of $PM_{2.5}$, SO_2, and NO_x in July for the three scenarios with ship emissions (2015, 2030 BAU, and 2030 ECA). All three pollutants show that the most heavily trafficked route is along the coast, especially on the eastern side of the PRD region.

3.2. Model Evaluation

Table 4 summarizes the model performance related to meteorological parameters. The 2-m temperature at Guangzhou between the simulated and observed had a correlation of 0.9 and an NMB of 0.3%. Small NMB values were also found at Shenzhen (0.2%) and at Zhaoqing (−0.3%), as well as in Hong Kong (−0.03%). The correlation coefficients between the observed and simulated for the 2-m temperature in the sites of Shenzhen, Zhaoqing and Hong Kong were 0.8, 0.7, and 0.8, respectively. The model slightly underestimated the relative humidity among all the four sites, and the correlation between the observed and the simulated was 0.50, 0.60, 0.52, and 0.65 and NMB of −16%, −12%, −1.6%, and −2.6%.

The model also underestimated the wind speed in Guangzhou, Shenzhen, and Hong Kong, with a correlation between the modeled and observed being 0.85, 0.80, and 0.83 and NMB of −15%, −36%, and −36%. The model, however, overestimated the wind speed at Zhaoqing, with a correlation of 0.5 and NMB of 32%. Figure 4 shows the comparison between the observed and modeled wind. The direction of each widget represents wind direction, and the color represents wind speed: the darker the color, the faster the wind. The length of each widget shows the number of hours that were observed or modeled within that direction where the wind comes from. We found that the southerly wind was the most dominant, indicating that wind most often blew from the ocean to the land. This result is consistent with the summer monsoon wind direction in China and confirms our expectation that ship emissions impact in land due to the dominant wind direction in July.

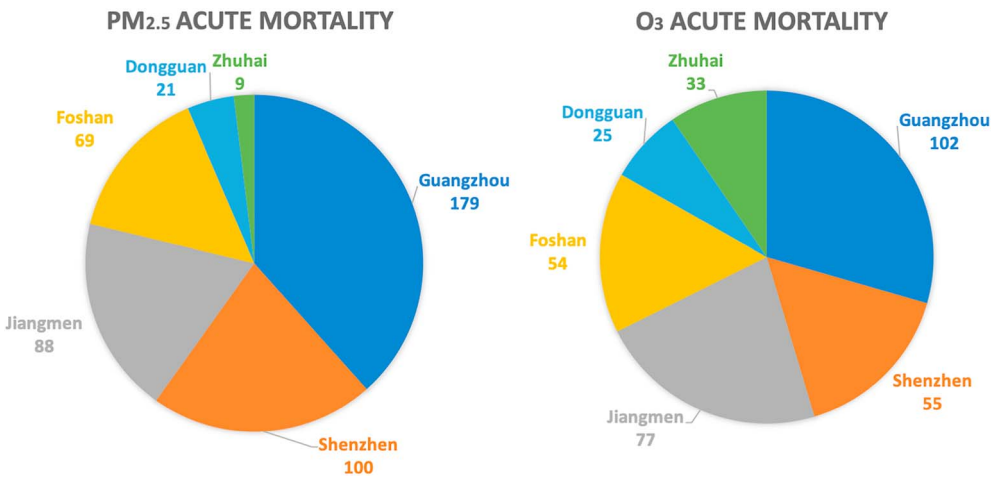

Figure 4. The comparison of wind speed and wind direction between the modeled and observed in July 2015; the length of each widget shows the number of hours that were observed or modeled within that direction, and the color of the widget shows the wind speed for each hour. The counts increase radially outward from the center.

Table 5 summarizes the model performance for two major health-related pollutants, $PM_{2.5}$ and O_3. We found that the model overestimated $PM_{2.5}$ concentrations in some cities, including Guangzhou and Shenzhen. This might be due to an underestimated wind speed and precipitation. As we mentioned earlier, we found that the modeled wind speed was smaller than the observed, which resulted in more stagnant air in some cities. Nevertheless, the $PM_{2.5}$ model performance for all cities still met the goal of MFB $\leq \pm 30\%$ and MFE $\pm 50\%$, suggested by Boylan and Russell (2006). The model performance of O_3 mixing ratios also met the goals of MFB ($\leq \pm 15\%$) and MFE ($\pm 35\%$). The comparison of modeled and observed $PM_{2.5}$ and O_3 (Figure S1), as well as SO_2 and NO_x concentrations (Figure S2), shows good agreement.

Table 5
Summary Statistics for Four Major Air Pollutant Concentrations Between Modeled and Observed in Nine Major Cities of the PRD Region in July 2015

Pollutant	City	NMB (%)	NME (%)	MFB (%)	MFE (%)	*r*	RMSE
$PM_{2.5}$	Guangzhou	193.3	197.4	20.3	21.5	0.5	81.6
	Shenzhen	245.3	245.3	24.3	24.3	0.3	62.6
	Zhuhai	86.6	98.4	10.1	14.5	0.6	26.8
	Foshan	53.6	71.8	7.9	12.4	0.5	36.2
	Zhongshan	195.2	195.3	20.8	20.8	0.4	58.2
	Jiangmen	209.1	211.8	18.7	19.5	0.4	54.1
	Dongguan	188.2	188.2	22.3	22.3	0.5	59.7
	Huizhou	199.5	199.9	24.5	24.6	0.5	49.1
	Zhaoqing	27.2	41.9	4.5	8.5	0.3	18.3
O_3	Guangzhou	−29.7	40.1	−6.2	10.5	0.5	69.1
	Shenzhen	−5.1	26.6	−0.3	6.1	0.5	37.2
	Zhuhai	−18.6	26.5	−2.9	5.7	0.8	43.4
	Foshan	−27.8	33.1	−7	8.6	0.7	53.1
	Zhongshan	−3.8	31.1	1.8	7.7	0.8	34.3
	Jiangmen	1.5	23.9	2.4	6.4	0.8	26.1
	Dongguan	−39.1	40.5	−10.8	11.5	0.7	73.3
	Huizhou	−3.2	19.8	0	5.1	0.8	23.2
	Zhaoqing	−26.8	30.5	−7	8.1	0.7	43.5

Note. PRD = Pearl River Delta; NMB = normalized mean bias; NME = normalized mean error; MFB = mean fractional bias; MFE = mean fractional error; RMSE = root-mean-square error.

Table 6
Monthly Average $PM_{2.5}$ and O_3 Concentrations for the Two Scenarios in July 2015: 2015 Without Ship and 2015 With Ship ($PM_{2.5}$ Unit: μg/m^3; O_3 unit: ppb)

City	2015 without ship $PM_{2.5}$	2015 with ship $PM_{2.5}$	2015 without ship O_3	2015 with ship O_3	Ship-caused $PM_{2.5}$ (%)	Ship-caused O_3 (%)
Guangzhou	72.06	74.21	56.55	58.2	2.15 (2.90%)	1.65 (2.80%)
Shenzhen	91.95	95.96	52.02	55.52	4.01 (4.20%)	3.50 (6.30%)
Foshan	70.02	71.68	57.25	59.01	1.66 (2.30%)	1.76 (3.00%)
Zhuhai	35.86	37.26	49.76	53.98	1.4 (3.80%)	4.22 (7.80%)
Dongguan	73.05	74.11	57.21	58.67	1.06 (1.40%)	1.46 (2.50%)
Zhaoqing	26.54	26.65	47.66	48.38	0.11 (0.40%)	0.72 (1.50%)
Huizhou	29.25	31.55	50.30	53.05	2.30 (7.30%)	2.75 (5.20%)
Jiangmen	31.18	32.25	49.51	51.37	1.06 (3.30%)	1.86 (3.60%)
Zhongshan	61.60	61.60	55.64	58.18	0.00 (0%)	2.54 (4.37%)
Hong Kong	51.16	57.27	48.50	54.30	6.12 (11.97%)	5.80 (11.96%)
Macao	51.21	54.95	49.09	55.19	3.75 (7.32%)	6.01 (12.42%)
PRD average	*42.60*	*44.03*	*51.19*	*53.09*	*1.43 (3.25%)*	*1.90 (3.71%)*

Note. The right two columns show the increased concentration due to ships and the percentage of the ambient pollutant concentration that was caused by ship in parentheses. PRD = Pearl River Delta.

3.3. Air Quality Impacts

3.3.1. Year 2015

Table 6 compares the $PM_{2.5}$ concentrations and O_3 mixing ratios under 2015 without ship (i.e., only land-based emissions) and 2015 With Ship scenarios, respectively. For these two scenarios, the monthly mean concentrations of $PM_{2.5}$ from the model were 42.6 and 44.0 μg/m^3 over the PRD region, respectively. Hong Kong was the individual city most impacted, with a 6.1-μg/m^3 increase in $PM_{2.5}$ concentrations due to ship emissions. We found that Shenzhen, Macao, Huizhou, and Guangzhou all had over 2.0-μg/m^3 increase in $PM_{2.5}$ concentrations due to ship emissions. For O_3, the monthly average 8-hr maximum mixing ratios for the PRD region were 51.2 and 53.1 ppb, for 2015 without ship and 2015 With Ship scenarios, respectively. The most impacted cities were Macao and Hong Kong, with 6.1- and 5.8-ppb increases in O_3. Zhuhai, Shenzhen, Huizhou, and Zhongshan were also greatly impacted by more than a 2.0-ppb increase of O_3. The reason Hong Kong and Macao are most impacted is mainly due to the increased emissions surrounding these cities and due to the wind direction (Figure 5).

Figure 5 presents the monthly average concentrations for 2015 without ship and 2015 With Ship scenarios, the increased concentrations due to ships in 2015, and the percentage of ship-related concentrations to the all-source concentrations for four major pollutants (i.e., O_3, $PM_{2.5}$, SO_2, and NO_x) within the finest resolution domain. For O_3, we found that the most affected area was the southeast of the PRD and the greatest increase (over 6-ppb increase) occurred above the sea. For $PM_{2.5}$, the largest impact due to ship emissions also took place in the southeast region, which is primarily ocean. The two short-lived pollutants, SO_2 and NO_x, increased by 10 μg/m^3 in the northern and eastern areas of the PRD, where Guangzhou, Shenzhen, and Hong Kong are all located.

We observed some areas where the $PM_{2.5}$ concentrations decreased after adding ship emissions. This is because the addition of ship emissions changed the WRF meteorological fields slightly, including the wind pattern, temperature, cloud formation, and precipitation. As an example, the wind pattern and temperature have indeed been altered after adding ship emissions (Figure S3). Those areas where we found decreased concentrations had an increase in wind speed that diffused pollution more rapidly. Zhongshan, for instance, had no change in $PM_{2.5}$ concentrations between the two scenarios (Table 6) due to some areas in the city observing lower $PM_{2.5}$ concentrations after we added ship emissions. On average, the ship-caused $PM_{2.5}$ concentration increase was negligible compared to other cities.

3.3.2. Year 2030

The pollutant ($PM_{2.5}$ and O_3) concentration differences between the BAU and ECA ship emissions under 2030 Constant and 2030 Projected scenarios are shown in Figure 6. These differences represent the potential air quality improvement that ECA could provide to the PRD cities in 2030. The monthly average $PM_{2.5}$

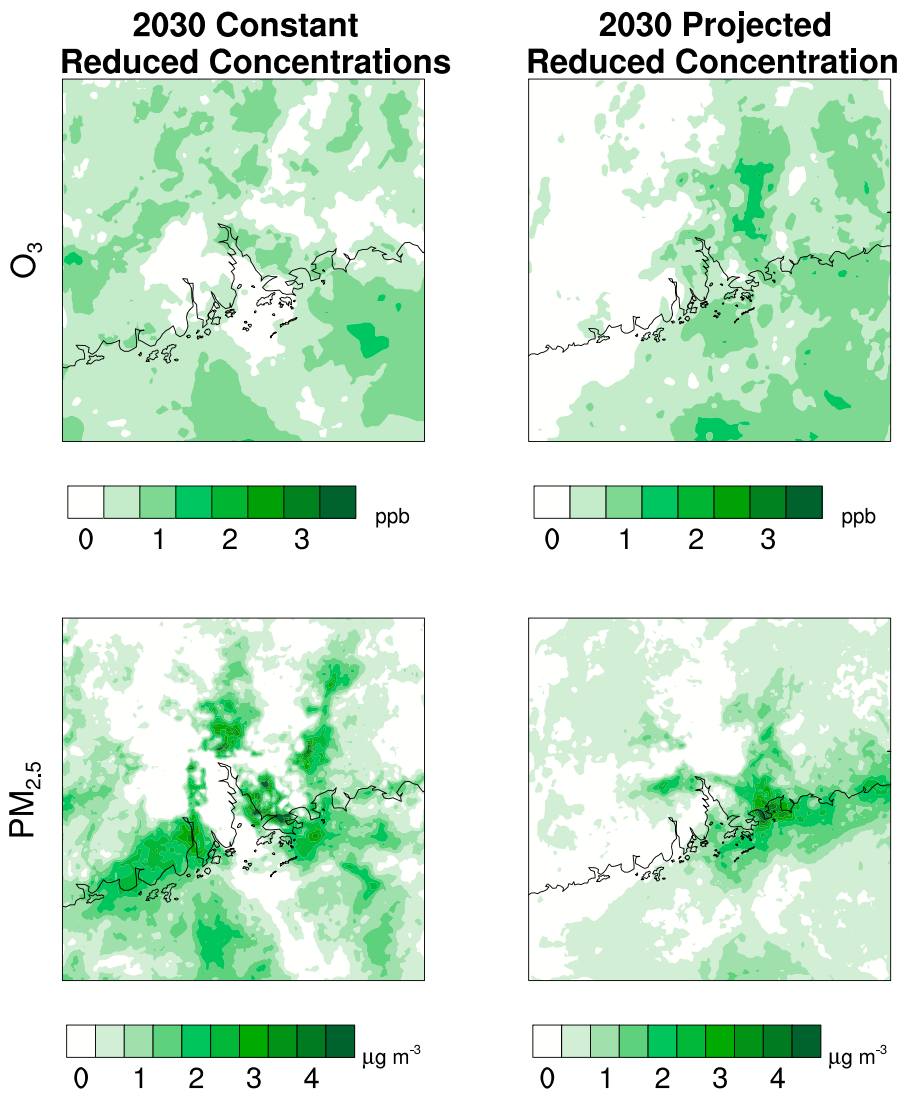

Figure 5. Four average pollutant ($PM_{2.5}$, O_3, SO_2, and NO_x) concentrations comparing two scenarios in July 2015: *2015 Without Ship* scenario (first column) and *2015 With Ship* scenario (second column); the change in concentrations after ship emissions is shown in the third column and the contributions of ship emission compared to other pollution sources are shown in the fourth column.

concentrations in the PRD region were 31.5 and 30.7 μg/m^3 for 2030 BAU Constant and 2030 ECA Constant, respectively. Hong Kong and Shenzhen would benefit the most if an ECA were implemented, as their monthly average $PM_{2.5}$ concentrations were projected to decrease by 1.9 and 1.3 μg/m^3, respectively. The monthly average O_3 mixing ratios in 2030 BAU Constant for the PRD region was 42.3 ppb and was fairly similar to that of 2030 ECA Constant (42.0 ppb). We found that Shenzhen and Dongguan would benefit the most from ECA, but the O_3 decreases in both cities were only 0.47 and 0.40 ppb, respectively. NO_x and SO_2 concentrations also decreased the most (over 2 μg/m^3) in the Eastern PRD, where Shenzhen, Dongguan, and Hong Kong are located.

The July average $PM_{2.5}$ greatly reduced to 12.3 μg/m^3 in 2030 BAU Projected and 12.0 μg/m^3 in 2030 ECA Projected from 44.0 μg/m^3 in 2015 With Ship. Shenzhen would benefit the most among all cities in PRD, as 1.5-μg/m^3 $PM_{2.5}$ concentration reduction was found due to ECA. The monthly average O_3 mixing ratio in *2030 BAU Projeced* for the PRD region was 38.5 ppb and in *2030 ECA Projeced* was 38.4 ppb, which indicated that ECA might not be as helpful in O_3 reduction under 2030 Projected scenario.

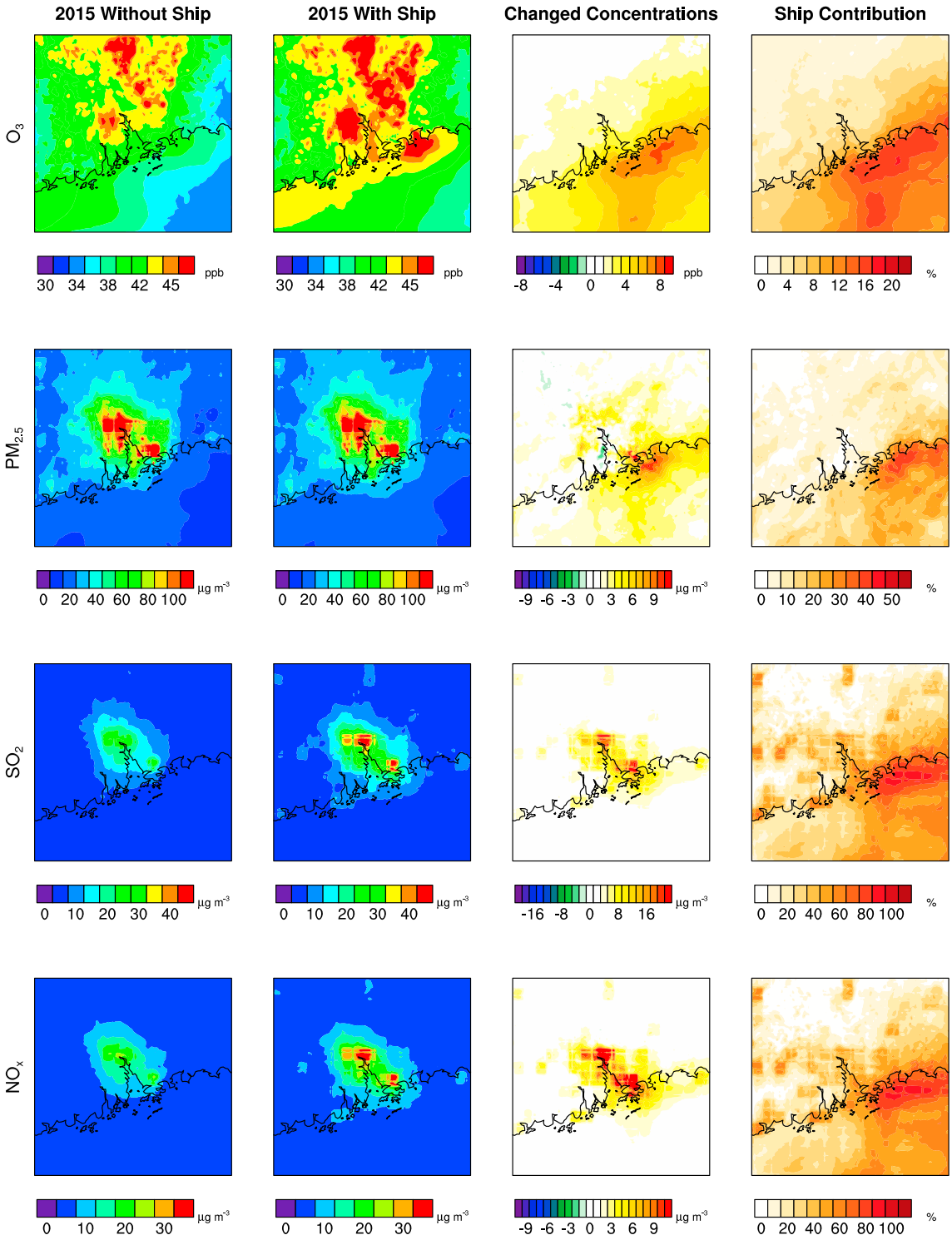

Figure 6. The reduced mean pollutant concentrations for O_3 and $PM_{2.5}$ from the BAU ship emissions to the ECA ship emissions under 2030 Constant and 2030 Projected scenario in July (units: ppb for O_3 and g/m^3 for $PM_{2.5}$).

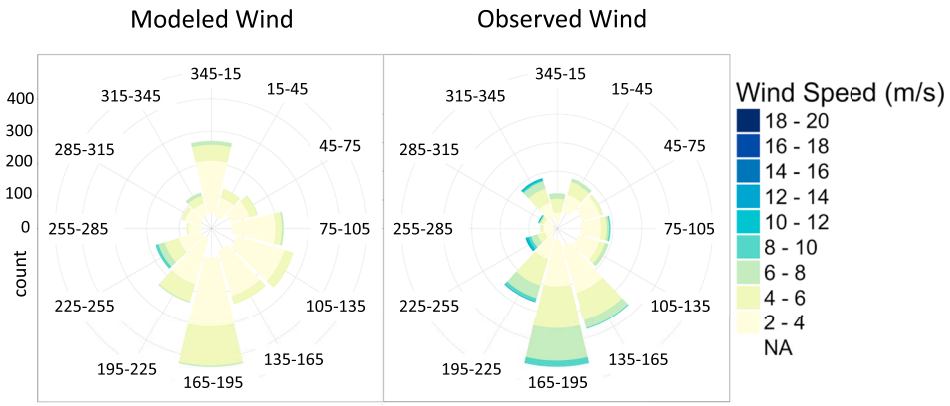

Figure 7. Premature mortality associated with short-term (acute) exposures to ship-related $PM_{2.5}$ and O_3 within six major cities in the Pearl River Delta region in 2015.

3.4. Health Impacts

3.4.1. Premature Mortality Associated With Acute Air Pollution Exposures in 2015

In 2015, we found that $PM_{2.5}$ concentrations due to ship emissions resulted in an estimated 466 (95% CI: 391, 545) acute premature deaths in six major cities in the PRD, including Guangzhou, Shenzhen, Jiangmen, Foshan, Dongguan, and Zhuhai. Acute premature deaths due to the exposure to O_3 from ship emissions were predicted to be 346 (95% CI: 268, 425; Figure 7). Acute mortality predictions are summarized in Table S5. Among the $PM_{2.5}$-related deaths, CVD deaths accounted for 54% of total deaths (251 cases, 95% CI: 207, 297) and RESP accounted for about 13% of total deaths (60 cases, 95% CI: 34, 84). On the other hand, ship-related O_3 increases were expected to result in 192 (95% CI: 136, 249) excess CVD deaths and 70 (95% CI: 49, 93) excess RESP deaths in 2015.

3.4.2. Premature Mortality Associated With Chronic Air Pollution Exposures in 2015

Ship-related chronic exposure to $PM_{2.5}$ resulted in a total of 2,085 (95% CI: 880, 2,929) predicted excess premature deaths in the PRD region due to IHD, COPD, LC, CEV, and RESP combined (Figure 8). We found the largest number of predicted excess premature deaths in Shenzhen (651 cases, 95% CI: 292, 868) for all-cause mortality, among the 11 cities. The reason that most predicted excess deaths were found in Shenzhen is due to its dense population and substantial contribution of ship emissions. There were also large numbers of predicted premature deaths in Hong Kong (370, 95% CI: 116, 608) and Guangzhou (346, 95% CI: 155, 462), since both are also highly populated cities. More than a hundred incidences of predicted excess premature mortality were also found in Foshan, Jiangmen, Dongguan, and Huizhou, due to ship emissions in 2015. We found that ship-related mortality accounted for 1.3% of total CEV, 0.8% of COPD, 0.8% of IHD, 0.4% of RESP, and 0.2% of LC in the PRD region.

Ship-related chronic exposure to O_3 resulted in a total of 852 (95% CI: 191, 1,310) predicted excess premature deaths in the PRD region due to CVD and RESP deaths combined (Figure 8). Among CVD death incidences (666 cases, 95% CI: 144, 1,088), approximately 48% (318, 95% CI: 66, 547) died from IHD. The lower-respiratory disease contributed to fewer predicted deaths than CVD as we predicted 186 (95% CI: 47, 222) excess deaths from the respiratory disease. Similar to $PM_{2.5}$, the increased O_3 also had the largest impact in three mega cities. Guangzhou, Shenzhen, and Hong Kong had the highest predicted chronic mortality from CVD and RESP. Outside of the three mega cities, we also predicted more than 50 excess deaths due to ship-induced chronic O_3 exposure in Dongguan, Foshan, and Huizhou. We found the greatest increase of O_3 mixing ratios by ship emissions in Zhuhai. However, due to its relatively small population size, the health impact due to ship-induced chronic O_3 exposure was less significant than the other cities.

3.4.3. Premature Mortality Associated With Chronic Air Pollution Exposures in 2030

Table 7 summarizes the detailed excess death incidence numbers for each health endpoint from both 2030 Constant and 2030 Projected scenarios. Under 2030 Constant scenario, we predicted 3,871 (95% CI: 1,360, 6,106) ship-related chronic excess deaths, where 3,019 (95% CI: 1,169, 4,786) of these were due to $PM_{2.5}$. Compared to 2015, the $PM_{2.5}$-related deaths due to ship emissions increased by 28%. Premature deaths due to O_3 exposure in 2030 also increased from 2015. In 2030, O_3-related mortality reached 957 (95% CI: 214, 1,482) deaths compared to 852 in 2015, resulting in a 12% increase. Under the 2030 Projected scenario, we

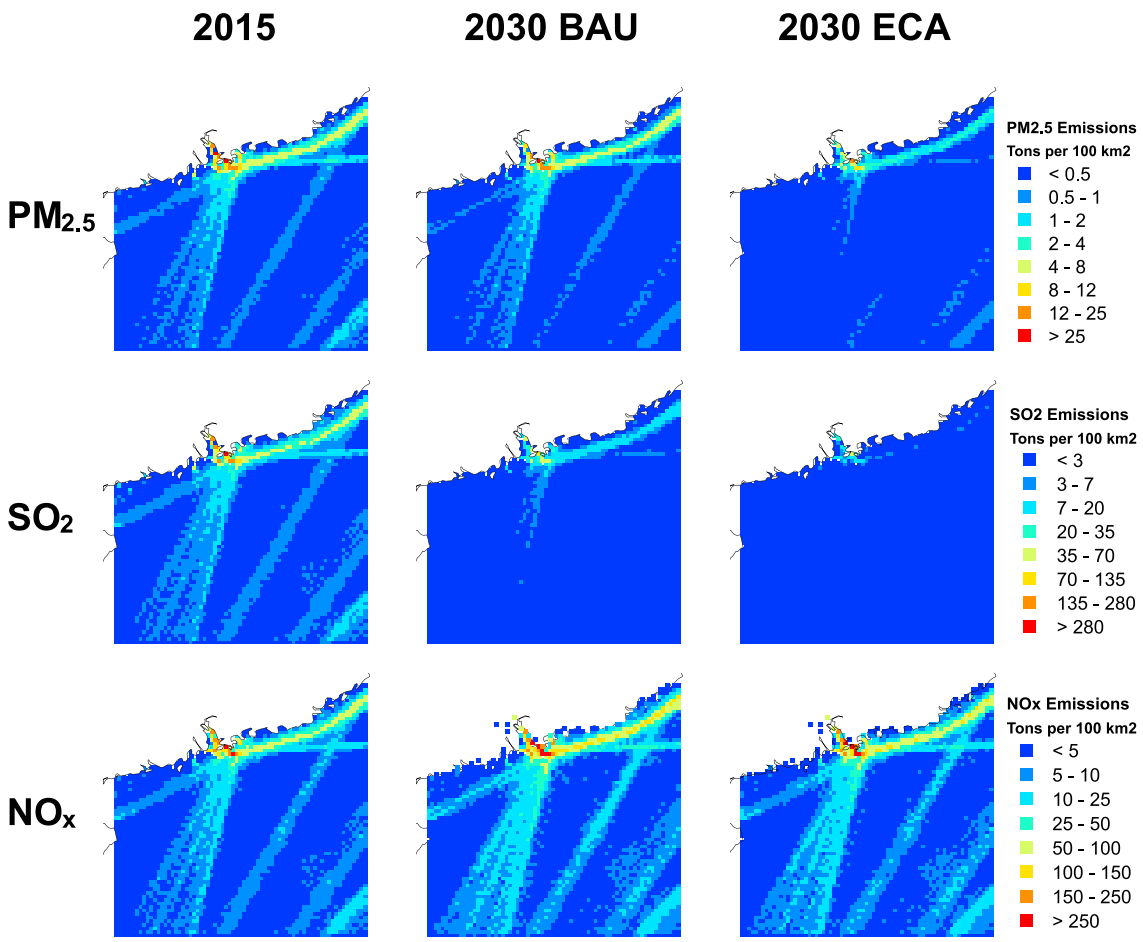

Figure 8. Premature mortality associated with long-term (chronic) exposures to ship-related $PM_{2.5}$ and O_3 in 2015.

found that the BAU ship emissions would result in 4,033 (95% CI: 1,548, 6,016) and 1,736 (95% CI: 501, 3,412) excess deaths due to chronic exposures to ship-related $PM_{2.5}$ and O_3, respectively. Together, excess deaths resulted in a total of 5,769 (95% CI: 2,049, 9,428) from the BAU ship emissions in the 2030 Projected scenario.

The potential health benefits provided by an ECA in 2030 were predicted by comparing $PM_{2.5}$ concentrations and O_3 mixing ratios with and without ECA implementation. We estimated the avoided premature deaths from implementing an ECA under both 2030 Constant and 2030 Projected scenarios. Under 2030 Constant scenario, implementing an ECA would avoid 811 (95% CI: 1,360, 1,280) $PM_{2.5}$-related deaths and 108 (95% CI: 24, 170) O_3-related deaths. These values were equivalent to a reduction of 27% and 11% of all-cause ship-related deaths in *2030 Constant BAU* scenario from $PM_{2.5}$ and O_3, respectively. Combining the total mortality from the two pollutants, an ECA would reduce ship-related premature deaths by 24% under 2030 Constant scenario.

Under 2030 Projected scenario, we found that an ECA would reduce all-cause $PM_{2.5}$-related deaths by 30% (1,194, 95% CI: 458, 1,770) and all-cause O_3-related premature deaths by 9.2% (160, 95% CI: 46, 318). In total, we estimated that an ECA would reduce ship-related premature deaths by 23%. The premature death reduction rates from an ECA were thus similar, under both 2030 Constant and 2030 Projected scenarios, highlighting the importance of regulating ship emissions, regardless of land emissions.

4. Discussion

In 2015, ship emissions were a major pollution source in the PRD region, accounting for 7%, 20%, and 17% of $PM_{2.5}$, SO_2, and NO_x, respectively, from all emissions. Ship emissions are expected to decrease significantly for both $PM_{2.5}$ and SO_2 in 2030 from the 2015 ship emission levels, even under 2030 BAU. There are two

Table 7
The Predicted 2030 BAU Death Incidences (Unit: Cases and 95% confidence intervals) and the Health Benefits (Unit: Cases and 95% confidence intervals and % death reduced) Brought by the ECA Implementation Under 2030 Constant and 2030 Projected Scenarios

Scenarios	$PM_{2.5}$	All cause	IHD	COPD	LC	CEV	RESP
2030 constant	BAU incidence (S2)	3,019 (1,169, 4,786)	838 (701, 1,312)	257 (111, 378)	272 (87, 387)	1,595 (385, 2,464)	56 (−115, 245)
	ECA benefits (S2–S3)	811 (317, 1,280)	225 (189, 351)	69 (29, 103)	72 (22, 104)	431 (103, 666)	13 (−26, 56)
	% Death reduced by ECA	26.9%	26.8%	26.8%	26.5%	27.0%	23.2%
2030 projected	BAU incidence (S4)	4,033 (1,548, 6,016)	1,612 (1,036, 2,163)	423 (18, 722)	399 (82, 657)	1,546 (521, 2,239)	54 (−109, 234)
	ECA benefits (S4–S5)	1,194 (458, 1,770)	495 (308, 661)	124 (4, 213)	117 (24, 193)	441 (155, 632)	16 (−33, 70)
	% Death reduced by ECA	29.6%	30.7%	29.3%	29.3%	28.5%	29.6%
Scenarios	O_3	All cause	CVD	RESP			
2030 constant	BAU incidence (S2)	957 (214, 1,482)	773 (167, 1,262)	184 (47, 220)			
	ECA benefits (S2–S3)	108 (24, 170)	94 (20, 153)	14 (4, 17)			
	% Death reduced by ECA	11.3%	12.2%	7.6%			
2030 projected	BAU incidence (S4)	1,736 (501, 3,412)	1,298 (356, 2,691)	439 (145, 720)			
	ECA benefits (S4–S5)	160 (46, 318)	127 (35, 264)	32 (11, 54)			
	% Death reduced by ECA	9.2%	9.8%	7.3%			

Note. BAU = Business As Usual; ECA = Emission Control Area; IHD = Ischemic heart disease; COPD = Chronic obstructive pulmonary disease; LC = Lung cancer; CEV = Cerebrovascular disease; RESP = Respiratory infection.

main reasons for the decrease. First, the fuel sulfur content is expected to reduce by 2030. Ships in 2015 were allowed to use fuels with a maximum sulfur content of 3.5% by mass. Beginning in October 2016, China implemented a DECA in the coastal PRD region that limited the maximum sulfur content of marine fuels to 0.5% for ships at berth, and since 2019, the DECA has been applied to all ships entering the PRD region. For 2030, we therefore assumed that the sulfur content of the fuel would be 0.5% within the DECA area. Second, beginning in 2020, the MARPOL Annex VI Regulation 14 will limit the maximum sulfur content of marine fuels to 0.5% globally. Reducing fuel sulfur content leads to BAU SO_2 and PM emissions being lower in 2030 compared to 2015, despite growth in shipping activity. In addition, lower SO_2 emissions result in lower secondary inorganic PM aerosol formation, further reducing ambient PM concentrations.

On the contrary, NO_x emissions from ships increased by 50 kt/year from 2015 to the 2030 BAU scenario due to a lack of strong control policies. The current global NO_x emission control, MARPOL Annex VI NO_x Tier II emission standards, applies to ships built on or after 1 January 2011. The NO_x Tier III emission standards only target ships built after 2016 and only when they travel inside the North American ECA. Under the 2030 BAU scenario, we therefore assumed no further NO_x control policies under the 2030 BAU ship emissions scenario. Because the ship size is expected to increase between 2015 and 2030, the incremental ship size in the 2030 BAU scenario led to higher NO_x emissions compared to the 2015 With Ship scenario.

Under the 2030 ECA Scenario, we found that an ECA would reduce $PM_{2.5}$ emissions by 57%, SO_x emissions by 76% and NO_x emissions by 13% compared to BAU ship emissions. $PM_{2.5}$ and SO_2 emission reductions result from lowering the maximum sulfur content in fuels from 0.5% to 0.1% inside the ECA. NO_x emissions were reduced by 13% from the BAU scenario due to NO_x Tier III emission standards for the newly constructed ships operating within the ECA. Compared to Tier II engine standards in the 2030 BAU, the NO_x Tier III emission standards are much more stringent, as mentioned earlier. Because we expect that an ECA would be established well before 2030, we assumed that new ships constructed on or after 1 January 2025 were subject to NO_x Tier III emission standards. Since ships built before 2025 would be grandfathered, the NO_x emission reduction benefit was limited, leading to only a moderate decrease in NO_x in 2030 compared to the BAU scenario. If the ECA NO_x requirements were to enter in force earlier than 2025, an ECA would result in greater NO_x reduction benefits in 2030.

We found that ship emissions increased air pollutant concentrations in the PRD region, espeically in the southeast. In 2015, ship emissions resulted in an average increase of 1.4 μg/m^3 for $PM_{2.5}$ and 0.9 ppb for O_3 in the PRD region. Cities such as Shenzhen, Dongguan, Huizhou, and Hong Kong observed over a 2-μg/m^3 increase of $PM_{2.5}$ and a 2 ppb increase of O_3. These results are consistent with Lv et al. (2018), who found that ship emissions elevated $PM_{2.5}$ concentrations by 1.6 μg/m^3 in the PRD region in 2015 and that Zhuhai

and Shenzhen were impacted more than Guangzhou by ship emissions. In the present study, the acute $PM_{2.5}$- and O_3-related deaths were 466 and 346, respectively, and the chronic premature deaths were 2,085 from ship-related $PM_{2.5}$ and 852 from ship-related O_3. We compared the health impact results with Liu et al. (2016), who found that 18,000 premature deaths were expected in 2013 in mainland China because of ship emissions. According to 2015 premature deaths due to ship emissions we expected in the PRD region (3,749 combined deaths from acute and chronic exposures), 21% of ship-related deaths in China took place within the cities of the PRD region. More recent study from Anenberg et al. (2019) shows that China in 2015 had 20,520 ship-related premature deaths. Combining our results with theirs, we found that around 18% of ship-related premature deaths in China occurred in PRD cities. The PRD, on average, accounted for 20% of ship-related premature deaths in China.

The concentration-response function is highly sensitive to the baseline incidence rate (y_0), as was illustrated in Guangzhou, which had the highest mortality from acute exposures but not from chronic exposures. For acute mortality, Guangzhou had the highest baseline incidence rate but for chronic mortality, we used the baseline incidence rate that was uniform across the entire PRD region in 2015. Similarly, the health end-point distribution was different for chronic mortality in Hong Kong, where respiratory disease had a higher percentage, while IHD, CEV, and COPD had a lower percentage than other cities (Figure 8). This was also because we adopted the separate baseline incidence rates for the Hong Kong population.

This study estimated the ECA health benefits from the reduction of $PM_{2.5}$ or O_3 exposures between the BAU and ECA ship emissions. Based on the long-term IER function, a cleaner air environment tends to have a higher RR than a more polluted environment. We found that an ECA could decrease $PM_{2.5}$ by 0.8 $\mu g/m^3$ and O_3 by 0.3 ppb in 2030 compared to BAU under the 2030 Constant scenario. On the other hand, ECA could only reduce $PM_{2.5}$ by 0.3 $\mu g/m^3$ and O_3 by 0.1 ppb under the 2030 Projected scenario. However, due to the 2030 BAU Constant resulting in much higher $PM_{2.5}$ concentrations and O_3 mixing ratios than the 2030 BAU Projected, an ECA would avoid less premature deaths under 2030 Constant (approximately 800 $PM_{2.5}$-related and 100 O_3-related premature deaths) than under 2030 Projected (approximately 1,200 $PM_{2.5}$-related and 160 O_3-related premature deaths). Despite the difference in absolute premature mortality numbers avoided between the two 2030 BAU scenarios, the combined mortality reduction rates due to ECA for both 2030 Constant and 2030 Projected scenarios were 23%. The expected health benefits from ECA were a nearly 30% reduction in premature mortality from $PM_{2.5}$ and 10% from O_3. Our results clearly indicated that ship emissions reduction policies produce health benefits, regardless of the land emissions.

In the North American ECA application (MEPC 59/6/5, 2009), researchers estimated that ship emissions in 2020 would lead to 5,100 to 12,000 deaths from both ship-related $PM_{2.5}$ and O_3 exposures. Among these, 3,700 to 8,300 lives could be saved by ECA implementation, by switching fuel from a maximum sulfur content of 2.7% to 0.1%. Our results show that 1,000–1,400 deaths can be saved from ship-related $PM_{2.5}$ and O_3 exposures by switching from 0.5% sulfur content to 0.1%. Considering the magnitude of the sulfur content reduction expected, it is reasonable that we observed smaller reduction in premature mortality in the PRD region compared to North America.

There are several limitations and uncertainties in this study. First, we only simulated air quality for 1 month and then applied the monthly results to estimate annual average concentrations to identify health effects due to ship emissions and the ECA implementation. The number of deaths might be overestimated, as our simulation period is chosen to be when the effects from ship emissions on land are the greatest based on the previous studies (Chen et al., 2018; Liu et al., 2018). However, the number of deaths might also be under-estimated because winter in the PRD has a higher $PM_{2.5}$ concentration in general, and the ship-induced concentrations could be more noteworthy. We hope to model multiple months in future studies to obtain more realistic health impacts. The choice of the year could also impact the study results. We chose the year of 2015 due to the data availability of both anthropogenic emissions and ship emissions. The precipitation in 2015 summer was, however, the highest among the year periods from 2011 to 2017 (WorldWeatherOnline, 2018). If we choose a low-precipitation year instead, the $PM_{2.5}$ concentrations would have been higher, had we modeled other reference years, because of less wet scavenging.

Second, the model in general overestimated $PM_{2.5}$ concentrations, as mentioned in the model evaluation section. One of the possible reasons is that the modeled wind had a lower wind speed than the observed. This could cause less diffusion of air pollution, resulting in stagnant polluted air. In addition, there is a large uncertainty in emissions inventories in China, as found in previous studies (Saikawa et al., 2017; Zhong et al.,

2016). For estimating chronic mortality, we used the IER function, which assumes a lower RR for greater ambient pollution levels. The overestimation of $PM_{2.5}$ concentrations in the model, therefore, might have resulted in lower premature mortality estimations.

Third, due to data availability, we ran the model with 2015 emissions for all nonship-related sources for the two 2030 scenarios. We also used the 2015 meteorological field to focus on the impacts of emissions on air quality. We thus focused our analysis on the relative concentrations and not on absolute concentrations for 2030. Future studies could investigate the impact of future climate on air quality as well.

Fourth, there remains a certain level of uncertainty in the estimates of future mortality. For example, the population data derived from the UN Department of Economic and Social Affairs have eight scenarios under different fertility and mortality patterns. The gridded population in 2030, however, simply extrapolated the 2015 gridded population by a scale factor, without considering any future migrations among cities. Similar uncertainty also exists in the baseline incidence rate in 2030. Furthermore, we used the same RR to estimate health benefits in 2030, which could also cause an overestimation. The medical science is advancing rapidly, so the actual RR in 2030 might be much lower than in 2015.

Last but not least, the chronic mortality model IER was built based on many assumptions. The model has to be further improved to estimate the mortality more accurately. In fact, the recent studies have developed alternative models other than the IER model. For example, Burnett et al. (2018) introduced a new one called the Global Exposure Mortality Model, which relaxes the contentious assumptions in the IER and builds the hazard ratio function based only on cohort studies of ambient air pollution. According to the study, the Global Exposure Mortality Model would predict much larger health benefits by reducing $PM_{2.5}$ than the IER model that we used in this paper. These are beyond the current scope of the paper but are nonetheless important future directions.

5. Conclusion

This study used WRF-Chem to estimate the impact of ship emissions on ambient air quality in China's PRD region, and we used concentration-response functions to quantify ship emissions-related premature mortality. In 2015, ship emissions resulted in more than 2,500 $PM_{2.5}$-related and 1,200 O_3-related premature deaths. In 2030, ship emissions would lead to more premature deaths, if no additional policies are considered.

Implementing an ECA results in substantial air quality and health benefits. Regardless of land emissions, the study found a combined 23% reduction in $PM_{2.5}$-related and O_3-related premature deaths because an ECA would significantly reduce SO_2, $PM_{2.5}$, and NO_x emissions from ships.

Our results show that ship emissions caused major environmental and health impacts in 2015 in PRD and will continue to do so in 2030. Implementing an ECA would improve air quality substantially and reduce premature mortality in the PRD region of China. We also found that an ECA is effective for PRD, regardless of land emissions.

Acknowledgments
The authors would like to thank the Health Effect Institute (HEI) for assisting with health benefits estimation and providing baseline mortality data. We also thank Dr. Qiang Zhang and Dr. Shuxiao Wang from Tshinghua University for providing the 2015 and 2030 land emission inventories. The authors also thank Dr. Lance Gunderson and Dr. Lance Waller for their helpful comments on the paper. This study was funded by the Energy Foundation China with support from Bloomberg Philanthropies. Gridded WRF-Chem simulation monthly averages for $PM_{2.5}$ and O_3 used in this study have been submitted to PANGAEA Data Archiving and will be available online.

Conflict of Interest

The authors declare no conflicts of interest relevant to this study.

References

Ackermann, I. J., Hass, H., Memmesheimer, M., Ebel, A., Binkowski, F. S., & Shankar, U. (1998). Modal aerosol dynamics model for Europe: Development and first applications. *Atmospheric environment*, *32*(17), 2981–2999.

Anenberg, S., Miller, J., Henze, D., & Minjares, R. (2019). A global snapshot of the air pollution-related health impacts of transportation sector emissions in 2010 and 2015 (Tech. Rep.): The International Council on Clean Transportation.

Boylan, J. W., & Russell, A. G. (2006). Pm and light extinction model performance metrics, goals, and criteria for three-dimensional air quality models. *Atmospheric environment*, *40*(26), 4946–4959.

Burnett, R., Chen, H., Szyszkowicz, M., Fann, N., Hubbell, B., Pope, C. A., et al. (2018). Global estimates of mortality associated with long-term exposure to outdoor fine particulate matter. *Proceedings of the National Academy of Sciences of the United States of America*, *115*(38), 9592–9597. https://doi.org/10.1073/pnas.1803222115

Burnett, R., Pope III, C. A., Ezzati, M., Olives, C., Lim, S. S., Mehta, S., et al. (2014). An integrated risk function for estimating the global burden of disease attributable to ambient fine particulate matter exposure. *Environmental health perspectives*, *122*(4), 397–403. https://doi.org/10.1289/ehp.1307049

Cai, S., Ma, Q., Wang, S., Zhao, B., Brauer, M., Cohen, A., et al. (2018). Impact of air pollution control policies on future PM2.5 concentrations and their source contributions in china. *Journal of environmental management*, *227*, 124–133.
Campling, P., Janssen, L., Vanherle, K., Cofala, J., Heyes, C., & Sander, R. (2013). Specific evaluation of emissions from shipping including assessment for the establishment of possible new emission control areas in European seas. Flemish Institute for Technological Research (VITO), Mol, BE.
Chang, J. C., & Hanna, S. R. (2004). Air quality model performance evaluation. *Meteorology and Atmospheric Physics*, *87*(1-3), 167–196.
Chen, D., Zhao, N., Lang, J., Zhou, Y., Wang, X., Li, Y., et al. (2018). Contribution of ship emissions to the concentration of PM2.5: A comprehensive study using AIS data and WRF/CHEM model in Bohai Rim Region, China. *Science of the Total Environment*, *610*, 1476–1486.
Comer, B., Olmer, N., Mao, X., Roy, B., & Rutherford, D. (2017). Black carbon emissions and fuel use in global shipping.
Corbett, J. J., Fischbeck, P. S., & Pandis, S. N. (1999). Global nitrogen and sulfur inventories for oceangoing ships. *Journal of Geophysical Research*, *104*(D3), 3457–3470.
Corbett, J. J., Winebrake, J. J., Green, E. H., Kasibhatla, P., Eyring, V., & Lauer, A. (2007). Mortality from ship emissions: A global assessment. *Environmental science & technology*, *41*(24), 8512–8518.
EPA (2012). Particle pollution and health. Tech. Rep.
Emmons, L. K., Walters, S., Hess, P. G., Lamarque, J.-F., Pfister, G. G., Fillmore, D., et al. (2010). Description and evaluation of the model for ozone and related chemical tracers, version 4 (MOZART-4).
Eyring, V., Isaksen, I. S., Berntsen, T., Collins, W. J., Corbett, J. J., Endresen, O., et al. (2010). Transport impacts on atmosphere and climate: Shipping. *Atmospheric Environment*, *44*(37), 4735–4771.
Frankel, E. G. (1989). Strategic planning applied to shipping and ports. *Maritime Policy & Management*, *16*(2), 123–132.
GDstats, G. S. B. (2016). Guangdong statistical yearbook. Retrieved from http://www.gdstats.gov.cn
Gong, S. (2003). A parameterization of sea-salt aerosol source function for sub-and super-micron particles. *Global Biogeochemical Cycles*, *17*(4), 1097. https://doi.org/10.1029/2003GB002079
Grell, G. A., Peckham, S. E., Schmitz, R., McKeen, S. A., Frost, G., Skamarock, W. C., & Eder, B. (2005). Fully coupled "online" chemistry within the WRF model. *Atmospheric Environment*, *39*(37), 6957–6975.
Guenther, A., Jiang, X., Heald, C., Sakulyanontvittaya, T., Duhl, T., Emmons, L., & Wang, X. (2012). The model of emissions of gases and aerosols from nature version 2.1 (MEGAN2. 1): An extended and updated framework for modeling biogenic emissions.
Huang, R., Chen, J., Wang, L., & Lin, Z. (2012). Characteristics, processes, and causes of the spatio-temporal variabilities of the East Asian monsoon system. *Advances in Atmospheric Sciences*, *29*(5), 910–942.
IWR (2016). U.S. army corps of engineers: Waterborne commerce statistics center. Retrieved from https://www.iwr.usace.army.mil/about/technical-centers/wcsc-waterborne-commerce-statistics-center/
Janssens-Maenhout, G., Crippa, M., Guizzardi, D., Dentener, F., Muntean, M., Pouliot, G., et al. (2015). Htap_v2. 2: A mosaic of regional and global emission grid maps for 2008 and 2010 to study hemispheric transport of air pollution. *Atmospheric Chemistry and Physics*, *15*(19), 11,411–11,432.
Jeong, J.-H., Shon, Z.-H., Kang, M., Song, S.-K., Kim, Y.-K., Park, J., & Kim, H. (2017). Comparison of source apportionment of PM2.5 using receptor models in the main hub port city of East Asia: Busan. *Atmospheric Environment*, *148*, 115–127.
Jerrett, M., Burnett, R. T., Pope III, C. A., Ito, K., Thurston, G., Krewski, D., et al. (2009). Long-term ozone exposure and mortality. *New England Journal of Medicine*, *360*(11), 1085–1095. https://doi.org/10.1056/NEJMoa0803894
Kurokawa, J., Ohara, T., Morikawa, T., Hanayama, S., Janssens-Maenhout, G., Fukui, T., et al. (2013). Emissions of air pollutants and greenhouse gases over Asian regions during 2000–2008: Regional emission inventory in Asia (REAS) version 2. *Atmospheric Chemistry and Physics*, *13*(21), 11,019–11,058.
Lin, H., Liu, T., Xiao, J., Zeng, W., Li, X., Guo, L., et al. (2016). Mortality burden of ambient fine particulate air pollution in six Chinese cities: Results from the pearl river delta study. *Environment international*, *96*, 91–97. https://doi.org/10.1016/j.envint.2016.09.007
Liu, H., Fu, M., Jin, X., Shang, Y., Shindell, D., Faluvegi, G., et al. (2016). Health and climate impacts of ocean-going vessels in East Asia. *Nature climate change*, *6*(11), 1037.
Liu, H., Jin, X., Wu, L., Wang, X., Fu, M., Lv, Z., et al. (2018). The impact of marine shipping and its DECA control on air quality in the Pearl River Delta, China. *Science of The Total Environment*, *625*, 1476–1485.
Lu, X., Chow, K.-C., Yao, T., Fung, J. C. H., & Lau, A. K. H. (2009). Seasonal variation of the land-sea breeze circulation in the pearl river delta region. *Journal of Geophysical Research*, *114*, D17112. https://doi.org/10.1029/2009JD011764
Lv, Z., Liu, H., Ying, Q., Fu, M., Meng, Z., Wang, Y., et al. (2018). Impacts of shipping emissions on $pm_{2.5}$ pollution in China. *Atmospheric Chemistry and Physics*, *18*(21), 15,811–15,824. https://doi.org/10.5194/acp-18-15811-2018
MOT (2016). Marine transport information for the year 2015. Ministry of Transport of the People's Republic of China. Retrieved from http://zizhan.mot.gov.cn/zfxxgk/bnssj/zhghs/201605/t20160506_2024006.html, http://xxgk.mot.gov.cn/jigou/zhghs/201704/t20170419_2976628.html
Morris, R., Koo, B., Wang, B., Stella, G., McNally, D., Loomis, C., et al. (2007). Technical support document for vistas emissions and air quality modeling to support regional haze state implementation plans. Novato, CA: Draft Final Report, ENVIRON.
NCEI (2018). Computer software manual. National Centers for Environmental Information, National Oceanic and Atmospheric Administration. Retrieved from http://gis.ncdc.noaa.gov/maps/ncei/cdo/hourly
Olmer, N., Comer, B., Roy, B., Mao, X., & Rutherford, D. (2017). Greenhouse gas emissions from global shipping, 2013–2015. The International Council on Clean Transportation.
Pope III, C. A., Burnett, R. T., Thun, M. J., Calle, E. E., Krewski, D., Ito, K., & Thurston, G. D. (2002). Lung cancer, cardiopulmonary mortality, and long-term exposure to fine particulate air pollution. *JAMA*, *287*(9), 1132–1141. https://doi.org/10.1001/jama.287.9.1132
SISI (2015). SISI releases 2030 China shipping development outlook. Shanghai International Shipping Institute. Retrieved 2019-01-28, from http://en.sisi-smu.org/index.php?c=article&id=13534 (accessed October 23, 2018).
Saikawa, E., Kim, H., Zhong, M., Avramov, A., Zhao, Y., Janssens-Maenhout, G., et al. (2017). Comparison of emissions inventories of anthropogenic air pollutants and greenhouse gases in China. *Atmospheric Chemistry and Physics*, *17*(10), 6393–6421.
Schell, B., Ackermann, I. J., Hass, H., Binkowski, F. S., & Ebel, A. (2001). Modeling the formation of secondary organic aerosol within a comprehensive air quality model system. *Journal of Geophysical Research*, *106*(D22), 28,275–28,293.
Shaw, W. J., Allwine, K. J., Fritz, B. G., Rutz, F. C., Rishel, J. P., & Chapman, E. G. (2008). An evaluation of the wind erosion module in Dustran. *Atmospheric Environment*, *42*(8), 1907–1921.
Sofiev, M., Winebrake, J. J., Johansson, L., Carr, E. W., Prank, M., Soares, J., et al. (2018). Cleaner fuels for ships provide public health benefits with climate tradeoffs. *Nature communications*, *9*(1), 406.

Stockwell, W. R., Middleton, P., Chang, J. S., & Tang, X. (1990). The second generation regional acid deposition model chemical mechanism for regional air quality modeling. *Journal of Geophysical Research*, *95*(D10), 16,343–16,367.

Tao, Y., Huang, W., Huang, X., Zhong, L., Lu, S.-E., Li, Y., et al. (2011). Estimated acute effects of ambient ozone and nitrogen dioxide on mortality in the Pearl River Delta of Southern China. *Environmental health perspectives*, *120*(3), 393–398.

Tao, J., Zhang, L., Cao, J., Zhong, L., Chen, D., Yang, Y., et al. (2017). Source apportionment of PM2.5 at urban and suburban areas of the Pearl River Delta region, South China—With emphasis on ship emissions. *Science of the Total Environment*, *574*, 1559–1570.

Tian, L., Ho, K.-F., Louie, P. K., Qiu, H., Pun, V. C., Kan, H., et al. (2013). Shipping emissions associated with increased cardiovascular hospitalizations. *Atmospheric environment*, *74*, 320–325.

UNCTAD (2018). Review of maritime transport 2017. Retrieved from http://unctad.org/en/PublicationsLibrary/rmt2018_en.pdf

Viana, M., Hammingh, P., Colette, A., Querol, X., Degraeuwe, B., de Vlieger, I., & van Aardenne, J. (2014). Impact of maritime transport emissions on coastal air quality in Europe. *Atmospheric Environment*, *90*, 96–105.

WHO (2013). Health effects of particulate matter (Tech. Rep. No. ISBN 978 92 8900001 7). World Health Organization. Retrieved from http://www.euro.who.int/__data/assets/pdf_file/0006/189051/Health-effects-of-particulate-matter-final-Eng.pdf

WSC (2014). Top 50 world container ports. World Shipping Council. Retrieved from http://www.worldshipping.org/about-the-industry/global-trade/top-50-worldcontainer-ports

Wiedinmyer, C., Akagi, S., Yokelson, R. J., Emmons, L., Al-Saadi, J., Orlando, J., & Soja, A. (2011). The fire inventory from NCAR (FINN): A high resolution global model to estimate the emissions from open burning. *Geoscientific Model Development*, *4*(3), 625.

Wild, O., Zhu, X., & Prather, M. J. (2000). Fast-j: Accurate simulation of in-and below-cloud photolysis in tropospheric chemical models. *Journal of Atmospheric Chemistry*, *37*(3), 245–282.

Winebrake, J. J., Corbett, J., Green, E., Lauer, A., & Eyring, V. (2009). Mitigating the health impacts of pollution from oceangoing shipping: An assessment of low-sulfur fuel mandates. *Environmental Science and Technology*, *43*(13), 4776–4782.

WorldWeatherOnline (2018). Guangdong statistical yearbook. Retrieved from https://www.worldweatheronline.com

Yau, P., Lee, S., Cheng, Y., Huang, Y., Lai, S., & Xu, X. (2013). Contribution of ship emissions to the fine particulate in the community near an international port in hong kong. *Atmospheric Research*, *124*, 61–72.

Zhang, Y.-L., & Cao, F. (2015). Fine particulate matter (pm 2.5) in China at a city level. *Scientific reports*, *5*, 14,884.

Zhang, Y., Yang, X., Brown, R., Yang, L., Morawska, L., Ristovski, Z., et al. (2017). Shipping emissions and their impacts on air quality in China. *Science of the Total Environment*, *581*, 186–198.

Zhong, M., Saikawa, E., Liu, Y., Naik, V., Horowitz, L. W., Takigawa, M., et al. (2016). Air quality modeling with WRF-CHEM v3. 5 in East Asia: Sensitivity to emissions and evaluation of simulated air quality. *Geoscientific Model Development*, *9*(3), 1201–1218.

Zhu, J. (2016). *China ports year book*. Beijing, China: China Ports.